

# The Distance to NGC 1316 (Fornax A) From Observations of Four Type Ia Supernovae<sup>1</sup>

Maximilian Stritzinger<sup>2,3,4</sup>, Christopher R. Burns<sup>5</sup>, Mark M. Phillips<sup>2</sup>, Gastón Folatelli<sup>6</sup>, Kevin Krisciunas<sup>7,3</sup>, ShiAnne Kattner<sup>8</sup>, Sven E. Persson<sup>5</sup>, Luis Boldt<sup>2</sup>, Abdo Campillay<sup>2</sup>, Carlos Contreras<sup>9</sup>, Wojtek Krzeminski<sup>2</sup>, Nidia Morrell<sup>2</sup>, Francisco Salgado<sup>2</sup>, Wendy L. Freedman<sup>5</sup>, Mario Hamuy<sup>6</sup>, Barry F. Madore<sup>5</sup>, Miguel Roth<sup>2</sup>, and Nicholas B. Suntzeff<sup>7</sup>

## ABSTRACT

The giant elliptical galaxy NGC 1316 (Fornax A) is a well-studied member of the Fornax Cluster and a prolific producer of Type Ia supernovae, having hosted four observed events since 1980. Here we present detailed optical and near-infrared light curves of the spectroscopically normal SN 2006dd. These data are used, along with previously published photometry of the normal SN 1980N and SN 1981D, and the fast-declining, low-luminosity SN 2006mr, to compute independent estimates of the host reddening for each supernova, and the distance to NGC 1316. From the three *normal* supernovae, we find a distance of  $17.8 \pm 0.3$  (random)  $\pm 0.3$  (systematic) Mpc for  $H_0 = 72$ . Distance moduli derived from

---

<sup>1</sup> This paper includes data gathered with the 6.5 meter Magellan telescope at Las Campanas Observatory, Chile.

<sup>2</sup>Carnegie Observatories, Las Campanas Observatory, Casilla 601, La Serena, Chile; mstritzinger@lco.cl.

<sup>3</sup>Dark Cosmology Centre, Niels Bohr Institute, University of Copenhagen, Juliane Maries Vej 30, 2100 Copenhagen Ø, Denmark; max@dark-cosmology.dk.

<sup>4</sup> The Oskar Klein Centre, Department of Astronomy, Stockholm University, AlbaNova, 10691 Stockholm, Sweden; max.stritzinger@astro.su.se.

<sup>5</sup>Observatories of the Carnegie Institution for Science, 813 Santa Barbara St., Pasadena, CA 91101, U.S.A.

<sup>6</sup>Universidad de Chile, Departamento de Astronomía, Casilla 36-D, Santiago, Chile.

<sup>7</sup> George P. and Cynthia Woods Mitchell Institute for Fundamental Physics and Astronomy, Texas A&M University, Department of Physics and Astronomy, College Station, TX 77843, U.S.A.

<sup>8</sup>Department of Astronomy, San Diego State University, San Diego, CA 92182-1221, U.S.A.

<sup>9</sup>Centre for Astrophysics & Supercomputing, Swinburne University of Technology, P.O. Box 218, Victoria 3122, Australia.

the “EBV” and Tripp methods give values that are mutually consistent to 4 – 8%. Moreover, the weighted means of the distance moduli for these three SNe for three methods agree to within 3%. This consistency is encouraging and supports the premise that Type Ia supernovae are reliable distance indicators at the 5% precision level or better. On the other hand, the two methods used to estimate the distance of the fast-declining SN 2006mr both yield a distance to NGC 1316 which is 25-30% larger. This disparity casts doubt on the suitability of fast-declining events for estimating extragalactic distances. Modest-to-negligible host galaxy reddening values are derived for all four supernovae. Nevertheless, two of them (SN 2006dd and SN 2006mr) show strong Na I D interstellar lines in the host galaxy system. The strength of this absorption is completely inconsistent with the small reddening values derived from the supernova light curves if the gas in NGC 1316 is typical of that found in the interstellar medium of the Milky Way. In addition, the equivalent width of the Na lines in SN 2006dd appear to have weakened significantly some 100-150 days after explosion.

*Subject headings:* galaxies: individual (NGC 1316) — supernovae: general — supernovae: individual (SN 1980N, SN 1981D, SN 2006dd, SN 2006mr)

## 1. INTRODUCTION

Type Ia supernovae (hereafter SNe Ia) are a powerful tool for measuring cosmological parameters and characterizing the nature of dark energy; for a contemporary review see Leibundgut (2008) and references therein. Given their importance, it is sensible when the opportunity presents itself, to test the consistency of distances afforded by SNe Ia. NGC 1316 (Fornax A) — a prolific producer of SNe Ia — offers such an opportunity, having hosted four Type Ia events since 1980. Here we present optical and near-infrared (NIR) light curves of the normal Type Ia SN 2006dd that cover the flux evolution from  $-10.5$  to  $+228$  days past  $B$  band maximum  $[T(B)_{\text{max}}]$ . These data are used, along with previously published optical and NIR photometry of SNe 1980N, 1981D and 2006mr, to determine independent measures of the distance to NGC 1316. Our analysis shows that the three *normal* SNe Ia do deliver consistent distances to NGC 1316. The fourth SN Ia in NGC 1316, SN 2006mr, was a fast-declining, sub-luminous event similar to the prototypical SN 1991bg (Filippenko et al. 1992; Leibundgut 1993; Turatto et al. 1996). Two methods are used to estimate the distance of NGC 1316 using this SN, but the overall agreement with the distance derived from the three normal SNe is poor.

NGC 1316 is a well-studied, radio-bright Morgan-D type galaxy in a peripheral area

of the Fornax I cluster. Detailed studies suggest that this galaxy is a remnant of an intermediate-age ( $\sim 3$  Gyr) merger (Schweizer 1980; Goudfrooij et al. 2001). The inner region is marked with a large dust lane while the outer region displays features related to tidal perturbations. Two giant radio lobes powered by a supermassive black hole extend from the center (Schweizer 1980; Geldzahler & Fomalong 1984; Nowak et al. 2008).

According to the infrared dust maps of Schlegel, Finkbeiner, & Davis (1998), the reddening due to dust within the Milky Way in the direction of NGC 1316 is  $E(B - V)_{\text{gal}} = 0.021$  mag. As we show below, the color excesses derived from the four SN Ia studied here, two of which lie in close proximity to the dust in the inner region of NGC 1316, suggest that they suffered relatively modest-to-negligible amounts of reddening.

The organization of this paper is as follows: § 2 describes the observational data set, § 3 presents the analysis where we estimate the host reddening and derive distances to NGC 1316 for each SN, § 4 discusses the strong interstellar Na I D absorption lines observed in the spectra of SNe 2006dd and 2006mr, and § 5 summarizes the conclusions.

## 2. The Observational Sample

The four SNe Ia that are the subject of this paper are SN 1980N, SN 1981D, SN 2006dd, and SN 2006mr. Figure 1 displays an image of NGC 1316 with the location of each SN indicated. SN 1980N was discovered on the rise by Maza & Wischnjewsky (1980) and later identified as a Type Ia event (Blanco et al. 1980; Prabhu 1981). Barely three months passed before a second SN, 1981D, was discovered in NGC 1316 (Cragg, Evans, & Maza 1981; Evans & Maclean 1982) and was also classified as a SN Ia (Menzies 1981). Optical spectra of SN 1980N published by Prabhu (1981) and Hamuy et al. (1991) reveal that this was a spectroscopically normal SN Ia. To our knowledge, a spectrum of SN 1981D has never been published, but the description of Menzies (1981) is consistent with it also having been a normal SN Ia.

Nearly a quarter of a century later, on 2006 June 19.2 UT, Monard (2006a) reported the appearance of SN 2006dd in the central region of the galaxy, that was spectroscopically classified as a young SN Ia (Salvo et al. 2006; Morrell et al. 2006). Less than five months later, Monard (2006b) discovered yet another SN in the central region of NGC 1316. Soon afterwards, this event, designated SN 2006mr, was reported to be a SN Ia similar to the fast-declining SN 1986G (Phillips et al. 2006).

Optical spectroscopy of SNe 2006dd and 2006mr was obtained during the course of the Carnegie Supernova Project (CSP; Hamuy et al. 2006). Table 1 contains a journal

of the spectroscopic observations, and the spectra themselves are shown in Figures 2 and 3. The six spectra of SN 2006dd displayed in Figure 2 range from  $-12$  to  $194$  days past  $T(B)_{\max}$ , and both the early- and late-phase spectra resemble that of a normal SN Ia. The spectroscopic sequence of SN 2006mr covers from  $-2$  to  $+63$  days past  $T(B)_{\max}$ , and displays a striking resemblance to the fast-declining, sub-luminous SN 1991bg (Filippenko et al. 1992; Leibundgut 1993; Turatto et al. 1996). This is demonstrated in the comparison of near- and post-maximum spectra shown in Figure 4. The spectra of both SN 2006dd and SN 2006mr exhibit conspicuous Na I D interstellar absorption at the redshift of NGC 1316. As discussed in § 4, there is evidence that the equivalent width of the Na I D absorption in SN 2006dd varied during the course of our spectroscopic coverage.

In the remainder of this section we discuss the optical and NIR broad-band observations of these four SN Ia.

## 2.1. Supernova 1980N

Nearly three weeks worth of optical photoelectric photometry was obtained by Landolt (Hamuy et al. 1991) and Olszewski (1982). A detailed analysis of these data is presented in Hamuy et al. (1991). The *BVRI* light curves cover the flux evolution from  $-0.8$  to  $+59.1$  days past  $T(B)_{\max}$ , and form a consistent set of photometry on the Landolt system.

To check the assumption made in Hamuy et al. (1991) that the host galaxy background had a negligible impact on the photometry, we measured the brightness of the host at the position of SN 1980N in high signal-to-noise images constructed from a series of frames obtained by the CSP at Las Campanas Observatory (LCO) throughout 2006. Prior to reassessing the background, we first determined new coordinates of SN 1980N. This was done in the following manner. Figure 1 of Hamuy et al. was scanned and converted to a FITS image from which the *XY* coordinates of a number of field stars were used to compute an astrometric world coordinate solution (WCS). Furnished with the WCS and the *XY* positions of SN 1980N, we then generated new 2000.0 coordinates of  $\alpha = 03^{\text{h}}23^{\text{m}}00^{\text{s}}.32$  and  $\delta = -37^{\circ}12'49''.9$ . We conservatively estimate the error in this position to be  $2\text{--}3''$  since an extrapolation of the astrometric solution was required. Note, however, that these new coordinates differ by  $10''$  in  $\alpha$  and  $2''$  in  $\delta$  from the position of SN 1980N given in the NASA Extragalactic Database (NED), which are from Tsvetkov & Bartunov (1993).

Next, at this location, a  $31''$  aperture was used to measure *B*- and *V*-band magnitudes from the 2006 stacked images of  $18.718 \pm 0.054$  mag and  $17.797 \pm 0.032$  mag, respectively. These values are  $\sim 3$  magnitudes fainter than the faintest SN measurement reported

in Hamuy et al. (1991). Moreover, Landolt probably used a  $16''$  aperture or smaller for his observations. This means that the galaxy light in his aperture was at least 60 times fainter than the SN, confirming that no background correction is necessary for the optical photometry of SN 1980N.

Elias et al. (1981) presented *JHK* light curves of SN 1980N that follow the flux evolution from day +5.3 to +72.2. These measurements were made with single channel photometers attached to telescopes at Cerro Tololo Inter-American Observatory (CTIO)<sup>10</sup> and LCO. The host galaxy contamination was estimated by sky observations made near the position of the SN. The final magnitudes were published on the CIT/CTIO system (Elias et al. 1982).

Plotted in Figure 5 are the optical and NIR light curves of SN 1980N.

## 2.2. Supernova 1981D

Walker & Marino (1982) published nine epochs of *B*- and *V*-band photoelectric photometry that ranged from day  $-4.6$  to  $+23.3$ . These observations were obtained on an unknown photometric system through a  $31''$  aperture, with no correction for the host galaxy light. As described above for SN 1980N, we measured the brightness of the host galaxy at the position of SN 1981D using the high signal-to-noise images taken in 2006. First, the 2000.0 coordinates of SN 1981D were determined to be  $\alpha = 03^{\text{h}}22^{\text{m}}38^{\text{s}}.38$  and  $\delta = -37^{\circ}13'57''.8$  using the same method described for SN 1980N. The error in this position is  $\sim 1''$ . Again, these new coordinates are substantially different ( $15''$  in  $\alpha$  and  $9''$  in  $\delta$ ) than those listed in NED (Tsvetkov & Bartunov 1993). The galaxy background at this position was measured in the 2006 stacked images with a  $31''$  aperture to be  $B = 15.230 \pm 0.010$  mag and  $V = 14.280 \pm 0.030$  mag. These robust measurements are brighter by 0.196 mag in *B* and 0.218 mag in *V* than those used in Hamuy et al. (1991) to correct the Walker & Marino (1982) photometry for background contamination. We therefore returned to the original Walker & Marino photometry and corrected for the new estimates of the background at the location of SN 1981D.

Seven epochs of NIR photometry of SN 1981D obtained at CTIO and LCO were also published by Elias et al. (1981). These *JHK* light curves follow the evolution from day +4.2 to +16.0, and are corrected for the host galaxy background light. The published magnitudes

---

<sup>10</sup>Cerro Tololo Inter-American Observatory, Kitt Peak National Observatory, National Optical Astronomy Observatories, operated by the Association of Universities for Research in Astronomy, Inc., (AURA), under cooperative agreement with the National Science Foundation.

are in the CIT/CTIO system.

The optical and NIR light curves of SN 1981D are plotted in Figure 6.

### 2.3. Supernova 2006dd

Thirteen epochs of optical and NIR imaging of SN 2006dd were obtained at CTIO with the SMARTS consortium 1.3 m telescope equipped with ANDICAM. The resulting  $BVRIJHK_s$  light curves nicely sample the flux evolution from  $-10.5$  to  $+55.4$  days past  $T(B)_{\max}$ . Additional optical ( $uBgVri$ ) imaging was carried out by the CSP with the Henrietta Swope 1.0 m telescope and SITe3 CCD camera at LCO. These light curves span from day  $+60.5$  to  $+228.2$ . A small amount of NIR imaging was also obtained by the CSP with the RetroCam imager on the Swope telescope after day  $+61$ . Complete details regarding the observing procedures used with ANDICAM, SITe3, and RetroCam can be found in Krisciunas et al. (2009), Hamuy et al. (2006), and Contreras et al. (2010).

All optical images were reduced in a standard manner including: (1) bias subtraction, (2) flat-field division, and (3) the application of a shutter time correction. NIR images were also reduced in a standard manner, consisting of (1) dark subtraction, (2) flat-field division, (3) sky subtraction, and (4) geometric alignment and combination of the dithered frames. Further details of the data reduction procedures are given in Krisciunas et al. (2009), Hamuy et al. (2006), and Contreras et al. (2010).

Photometry of SN 2006dd was computed differentially with respect to a sequence of stars in the field of NGC 1316. The local sequence used to compute optical photometry from the ANDICAM images consists of four stars calibrated to observations of the PG1657 field (Landolt 1992) obtained on five photometric nights. Final magnitudes for these stars are given in Table 2. For the SITe3  $uBgVri$  imaging, we adopted the same local sequence established in Contreras et al. (2010, see their Table 3) to compute photometry of SN 2006mr (see below). This sequence was calibrated to the Landolt (1992)  $BV$  and Smith et al. (2002)  $ugri$  systems through standard star observations obtained over the course of four photometric nights.

Three stars are in common between the two different local sequences. Two of these stars have consistent  $B$  and  $V$  magnitudes, however the faintest of these three stars exhibits a difference of up to nearly a tenth of a magnitude. The average difference between the three common stars is found to be 0.038 mag and 0.042 mag in  $B$  and  $V$ , respectively.

Prior to computing final photometry, template images of NGC 1316 were subtracted at

the location of SN 2006dd from all science images. The templates were obtained well after the SN faded, with the identical telescope/instrument/filter combinations used to obtain the science images. Finally, point spread function (PSF) photometry was computed from the template-subtracted science images.

To facilitate the analysis of the light curves (see § 3), we elected to forego the application of color corrections, and computed the ANDICAM optical photometry in the *natural* system of the 1.3 m telescope. To accomplish this, it was necessary to convert the optical magnitudes listed in Table 2 from the standard to the natural system using the following equations:

$$B_{\text{nat}} = B_{\text{std}} - CT_B \cdot (B_{\text{std}} - V_{\text{std}}) \quad (1)$$

$$V_{\text{nat}} = V_{\text{std}} - CT_V \cdot (B_{\text{std}} - V_{\text{std}}) \quad (2)$$

$$R_{\text{nat}} = R_{\text{std}} - CT_R \cdot (V_{\text{std}} - R_{\text{std}}) \quad (3)$$

$$I_{\text{nat}} = I_{\text{std}} - CT_I \cdot (V_{\text{std}} - I_{\text{std}}). \quad (4)$$

These transformations adopt the mean color terms derived from ANDICAM observations of standard fields obtained during seven photometric nights between June 22 to August 25, 2006. Specifically, the color terms used are  $CT_B = +0.091 \pm 0.014$ ,  $CT_V = -0.019 \pm 0.007$ ,  $CT_R = +0.031 \pm 0.011$ , and  $CT_I = -0.032 \pm 0.012$ . The resulting ANDICAM photometry of SN 2006dd on the natural system of the 1.3-m telescope is given in Table 3.

Likewise, the LCO optical photometry of SN 2006dd was computed in the natural system of the Swope 1 m telescope + SITe3 camera following the procedures detailed in Contreras et al. (2010). Final magnitudes are listed in Table 4.

The NIR photometry of SN 2006dd obtained with ANDICAM and RetroCam was reduced in a similar fashion to the optical data. The  $JHK_s$  magnitudes of star CSP02 of the ANDICAM local sequence were calibrated directly to the Persson et al. (1998) NIR photometric system via observations of the standard stars P9109, P9150, and P9172 assuming no color term. This star is also in the 2MASS catalog, and we find that our magnitudes are between 0.02 to 0.06 mag brighter than their 2MASS values. Table 2 contains the final  $JHK_s$  magnitudes of star CSP02 in the Persson standard system. For the CSP RetroCam observations on the Swope 1 m telescope, we adopted the local NIR sequence for SN 2006mr published by Contreras et al. (2010, see their Table 3). This sequence was calibrated to the Persson et al. (1998) system through standard star observations obtained over the course of 15 photometric nights. Final NIR magnitudes for SN 2006dd in the natural systems of the 1.3 m and Swope 1 m telescope are given in Table 3.

Plotted in Figure 7 are the early phase optical and NIR light curves of SN 2006dd computed from the ANDICAM and RetroCam images. In Figure 8, the full set of  $BVri$  observations obtained at CTIO and LCO are shown together. “S-corrections” (Suntzeff 2000; Stritzinger et al. 2002) calculated using an updated version of the Hsiao et al. (2007) SN Ia spectral template have been applied to the ANDICAM observations to place them on the natural system of the Swope telescope. Although there is no overlap between the two sets of observations, the agreement is generally quite good.

The later phase light curves of SN 2006dd are amongst the most densely sampled yet obtained for a SN Ia out to day +230. Linear least-squares fits to the photometry after 150 days past  $T(B)_{\max}$  yield decline rates of 1.6, 1.6, 2.2, and 1.5 mag per hundred days in  $B$ ,  $V$ ,  $r$ , and  $i$ . These decline rates are marginally steeper than what has been documented in most other SNe Ia (Lair et al. 2006).

## 2.4. Supernova 2006mr

Detailed optical ( $uBgVri$ ) and NIR ( $YJH$ ) light curves of SN 2006mr have recently been published by the CSP (Contreras et al. 2010). The photometry spans from  $-4.3$  to  $+96.6$  days past  $T(B)_{\max}$ , and is on the Swope telescope natural system. SN 2006mr is one of several low-luminosity, fast-declining events contained in the first CSP data release of SNe Ia, and a detailed analysis of these data is presented in Folatelli et al. (2010).

# 3. Analysis

## 3.1. Light Curve Fitting

To estimate the reddening and distance to each SN Ia, we made use of the template light curve fitting package SNooPy [SuperNovae in object-oriented Python; Burns et al. (2010)]. A description of SNooPy and the construction of its template light curves is presented in Folatelli et al. (2010); here we briefly summarize.

SNooPy is based on a modified version of the Prieto method (Prieto et al. 2006), and contains optical ( $uBgVri$ ) and NIR ( $YJH$ ) template light curves built from well-observed SNe Ia obtained during the first four campaigns of the CSP. To fabricate the templates, cubic spline functions are fitted to each light curve (corrected for time dilation) and estimates of the peak magnitude,  $m_{\max}$ , the time of maximum,  $T_{\max}$ , and the decline rate param-



eter,  $\Delta m_{15}(B)$ , are extracted.<sup>11</sup> The values of these parameters are then combined with the Hsiao et al. (2007, 2010) SN spectral templates, and K-corrections are computed (see Freedman et al. 2009, § 5.1 for more details). The K-corrected photometry then undergoes another round of spline fits yielding revised estimates of  $m_{\max}$ ,  $T_{\max}$ ,  $\Delta m_{15}(B)$ , as well as a complete covariance matrix for the light curve parameters. Each filter’s K-corrected and time-dilation-corrected photometric data now form a 2D surface in a 3D  $[t-T_{\max}, m-m_{\max}, \Delta m_{15}(B)]$  space, which can generate for any given  $\Delta m_{15}(B)$  a template light curve by simply interpolating within this surface. This manner of interpolation is the main difference from the original Prieto method, and boils down to SNooPy producing templates by doing 2D interpolating among the original data points of the SNe rather than using the weighted average of the 1D spline functions.

The scarcity of published  $K_s$ -band light curves with decent pre-maximum sampling hinders our ability to build suitable templates for this particular passband. We therefore fit the observed photometry with the  $K_s$ -band polynomial template presented by Krisciunas, Phillips & Suntzeff (2004), multiplied by an appropriate stretch value that is related to  $\Delta m_{15}(B)$  (see Folatelli et al. 2010, Equation 1).

As the template light curves built into SNooPy are on the natural system of the Swope telescope, it is necessary to transform (when appropriate) the SN photometry to be fit by SNooPy to this system. This was accomplished through the application of time-dependent corrections computed synthetically from template SN spectra (Suntzeff 2000). Done correctly, these “S-corrections” also require an accurate idealization of the total response function of the telescope/instrument/filter combination used to obtain the science images. We therefore carefully constructed model passbands where necessary, and then, following the method presented in Stritzinger et al. (2002), combined these passbands with a library of template SN spectra (Hsiao et al. 2007, 2010) to compute the S-corrections. As mentioned in § 2.2, it is not known in which photometric system the  $B$ - and  $V$ -band light curves of SN 1981D are published. In what follows, we simply assume that they are on a photometric system similar to that of the Swope telescope, i.e., assume  $B$  and  $V$  are in the CSP natural system and require no S-corrections. If we were to assume these bands are on the standard Landolt system, the estimated distance modulus to NGC 1316 decreases by only  $\sim 0.002$  mag.

---

<sup>11</sup> $\Delta m_{15}(B)$  is defined as the difference between the  $B$ -band magnitude at peak and 15 days later. This parameter correlates with the absolute peak magnitude of a SNe Ia in the sense that more luminous events have smaller decline rates (Phillips 1993). Because a single value of  $\Delta m_{15}(B)$  is used in SNooPy to parameterize all the filters of a SN Ia, the values reported here will differ somewhat from the value one would get by measuring it directly from the decline of the  $B$ -band light-curve alone.

SNooPy has two different models for performing the light curve fits. In the “max” model, the observed magnitudes of the SN in each filter are fitted simultaneously according to the following equation:

$$m_X[t - T(B)_{\max}] = T_X[(t - T(B)_{\max})/(1 + z), \Delta m_{15}(B)] + m_X^{\max}. \quad (5)$$

The input data for this model are the redshift of the host galaxy,  $z$ , the observed magnitudes in filter  $X$ ,  $m_X$ , as a function of time,  $t$ , corrected for Galactic reddening assuming a Cardelli, Clayton, & Mathis (1989) reddening law with  $R_V = 3.1$  and K-corrected as described in Folatelli et al. (2010). The fitting of the photometry to the SNooPy template functions,  $T_X$ , is performed simultaneously in all observed bands through  $\chi^2$  minimization, yielding as final output parameters:  $T(B)_{\max}$ ,  $\Delta m_{15}(B)$ , and the peak magnitudes,  $m_X^{\max}$ , in each filter. The results of these fits for SNe 1980N, 1981D, and 2006dd are given in Table 5 and plotted as dashed lines on top of the observed photometry in Figures 5–7. The quoted uncertainties for the fit parameters were derived from the covariance matrix of the best template fits, scaled such that  $\chi^2_{\nu} = 1$ .

Unfortunately, SNooPy does not yet do a very good job of fitting the light curves of fast declining SNe Ia. Hence, for SN 2006mr, we take the light curve parameters given by Folatelli et al. (2010) that were estimated through the use of spline fits. These values are reproduced in Table 5. Note that, in this case, the parameter,  $\Delta m_{15}(B)$ , is a direct measurement of the decline rate of the  $B$  light curve.

Using the “EBV” model in SNooPy, the light curve data are fit to the following alternative model:

$$m_X[t - T(B)_{\max}] = T_X[(t - T(B)_{\max})/(1 + z), \Delta m_{15}(B)] + M_X^{\max}[\Delta m_{15}(B)] + \mu_o + R_X^{\text{Host}} \cdot E(B - V)_{\text{Host}} \quad (6)$$

Here  $M_X^{\max}[\Delta m_{15}(B)]$  is the unreddened absolute magnitude at maximum in band  $X$  of a SN Ia with a decline rate of  $\Delta m_{15}(B)$ ,  $E(B - V)_{\text{host}}$  is the reddening produced in the host galaxy, and  $R_X^{\text{host}}$  is the total-to-selective absorption coefficient. For the values of  $M_X^{\max}[\Delta m_{15}(B)]$  and  $R_X^{\text{host}}$ , we adopt the recommended calibration from Burns et al. (2010), which uses a subsample of unreddened SNe Ia from Folatelli et al. (2010) and excludes the two very red SNe Ia SN 2006A and SN 2006X. Note that this calibration assumes  $H_o = 72 \text{ km s}^{-1} \text{ Mpc}^{-1}$ . Simultaneously fitting the light curve data in all filters yields final output

values of  $T(B)_{\max}$ ,  $\Delta m_{15}(B)$ ,  $E(B - V)_{\text{host}}$ , and the distance modulus,  $\mu_0$ . Best-fit models for SNe 1980N, 1981D, and 2006dd derived from Equation 6 are plotted as smooth curves in Figures 5–7, and the pertinent fit parameters are given in Tables 6 and 7. The quoted values of  $\mu_0$  listed in Table 7 were computed by solving for the single value of  $\mu_0$  that minimizes the  $\chi^2$  for all of the light curves. As the Burns et al. (2010) relations are only valid for SNe Ia with decline rates in the range  $0.7 < \Delta m_{15}(B) < 1.7$ , the EBV model cannot be applied to the fast-declining SN 2006mr.

A peculiarity of the Burns et al. (2010) calibration is its low value for the host-galaxy’s total-to-selective absorption coefficient,  $R_V^{\text{host}} \sim 2$ . Indeed, most of the derived values of  $R_V^{\text{host}}$  from Folatelli et al. (2010) are very low compared to the Milky Way. It can be argued that if interstellar dust in these hosts is anything like that found in the Milky Way or in the Small and Large Magellanic clouds, such a value of  $R_V^{\text{host}}$  is physically unreasonable. However, when considering only the ratio of the color excesses in different filters, Folatelli et al. (2010) derive an average value of  $R_V^{\text{host}}$  that is consistent with  $R_V^{\text{host}} = 3.1$ . Nevertheless, imposing a larger value of  $R_V^{\text{host}}$  results in poorer quantitative fits to the light curves of those SNe Ia in the calibration sample with large extinctions, as well as a much larger dispersion in the derived Hubble diagram. A simple explanation is that there is another physical process, other than dust, causing intrinsically red SNe to be dimmer and that this process is uncorrelated with  $\Delta m_{15}(B)$ . The *empirical* fact remains that using a small value of  $R_V^{\text{host}}$  results in better standard candles, especially for SNe Ia that occur in massive host galaxies such as NGC 1316 (Sullivan et al. 2010).

### 3.2. Host Galaxy Reddening

The  $E(B - V)$  color excesses derived from the SNooPy EBV method (listed in the second column of Table 6) indicate that the three “normal” events, SNe 1980N, 1981D, and 2006dd, suffered modest to negligible amounts of host galaxy reddening. As previously mentioned, the calibration from Burns et al. (2010) is not applicable to the fast-declining, intrinsically-red SN 2006mr, and so its host galaxy reddening cannot be estimated via the SNooPy fits. However, Lira (1995) found that the  $(B - V)$  colors of SNe Ia at 30–90 days past  $V$  maximum evolve in a nearly identical fashion, offering an alternative method for measuring host galaxy reddening. Lira’s sample included only one fast-declining event (SN 1991bg), but Taubenberger et al. (2008, see also Garnavich et al. (2004)) studied a sample of eight fast-declining events and concluded that they all follow reasonably well the Lira relation (Lira 1995). Applying the Lira relation to SN 2006mr, Folatelli et al. (2010) derived a color excess of  $E(B - V)_{\text{host}} = -0.025 \pm 0.013$  mag. This estimate indicates that SN 2006mr

suffered essentially no host reddening. For completeness, we have applied the Folatelli et al. (2010) calibration of the Lira law to the two normal events with sufficient late-time coverage, SNe 1980N and 2006dd. The results (given in the third column of Table 6) are fully consistent with the modest reddening values yielded by SNooPy.

An alternative way to estimate the host reddening is through the comparison of “zero-reddening” loci to the observed  $V$  minus NIR colors of each supernova. Krisciunas et al. (2000) have provided such a set of low zero-reddening loci, but these were fabricated in part with photometry of SNe 1980N and 1981D. This motivated us to construct a new set of zero-reddening loci based on photometry of the well-observed SN 2001el (Krisciunas et al. 2003). To obtain these, the observed  $V$  minus NIR colors of SN 2001el were dereddened using the following color excesses:  $E(V - J) = 0.450$  mag,  $E(V - H) = 0.499$  mag and  $E(V - K) = 0.530$  mag. These values were derived through comparison of the color evolution of SN 2001el to that of its low reddened twin SN 2004S, adopting the Galactic reddening law of Cardelli, Clayton, & Mathis (1989) as modified by O’Donnell (1994) (hereafter referred to as the “CCM+O” law) with an  $R_V = 3.1$  for the Galactic reddening correction, and an  $R_V^{\text{host}} = 2.15$  for the host reddening portion (see Krisciunas et al. 2007, for details).

Plotted in Figure 9 are the  $(V - J)$ ,  $(V - H)$  and  $(V - K)$  color curves of the four SNe in NGC 1316, and the new zero-reddened loci. Also included for comparison are the loci of Krisciunas et al. (2000). When compared to the new loci derived from SN 2001el, each color combination of SN 1980N and SN 1981D yields slightly negative color excesses, suggesting they suffered essentially no host extinction. On the other hand, the best fit locus to each color curve of SN 2006dd give colors excesses of  $E(V - J) = 0.201 \pm 0.169$  mag,  $E(V - H) = 0.259 \pm 0.129$  mag and  $E(V - K) = 0.253 \pm 0.142$  mag, which correspond to a weighted average reddening of  $E(B - V) = 0.093 \pm 0.038$  mag. When converting the  $V$  minus NIR color excesses to  $E(B - V)$ , we used reddening law coefficients from Table 13 (columns 4 and 5) of Folatelli et al. (2010), along with Equation A4 of Krisciunas et al. (2006) and an  $R_V^{\text{host}} = 3.2 \pm 0.31$ . This value of  $R_V^{\text{host}}$  is the favored value obtained through the comparison of  $V$  minus NIR color excess to  $E(B - V)$  of SNe Ia with low-to-moderate reddening values (see Folatelli et al. 2010, Figure 13). The specific conversion formulae are  $E(B - V) = 0.435 \cdot E(V - J)$ ,  $E(B - V) = 0.382 \cdot E(V - H)$ , and  $E(B - V) = 0.354 \cdot E(V - K)$ . If we instead adopt an  $R_V^{\text{host}} = 1.7 \pm 0.05$ , corresponding to the reddening law value derived for a sample of moderate-to-low and highly reddened SNe Ia (see Folatelli et al. 2010, Figure 13), the  $V$  minus NIR color excesses derived from the zero-reddened loci of SN 2001el imply a weighted average reddening of  $E(B - V) = 0.156 \pm 0.057$  mag.

Recently, Krisciunas et al. (2009) noted that the  $(V - H)$  and  $(V - K)$  colors of fast declining SNe Ia are also remarkably uniform after  $t \sim +30$  days, and very similar to the

unreddened colors of mid-range decliners. As shown in Figure 9, the  $(V - H)$  color evolution of SN 2006mr is much redder than that of SN 2006dd until  $t \sim +25$  days, highlighting the intrinsically red nature of the fast-declining SNe Ia. After  $t \sim +25$  days, the colors of the normal SNe are similar, although not identical. As NIR light curves of more fast-declining SNe Ia are obtained, it will be interesting to see if a “NIR Lira law” exists which can be used to derived host galaxy reddening over the entire observed range of decline rates of SNe Ia.

In summary, we find (i) the EBV method and the Lira relation indicate that SN 1980N is perhaps slightly reddened [ $E(B - V)_{\text{host}} = 0.06$  mag] while the  $V$  minus NIR colors suggest no host reddening, (ii) the EBV method indicates SN 1981D has a color excess of  $E(B - V)_{\text{host}} = 0.08$  mag, while the  $V$  minus NIR colors indicate no reddening, (iii) the EBV method and the NIR colors show SN 2006dd suffered a small amount of reddening in the range  $E(B - V)_{\text{host}} \sim 0.04\text{--}0.09$  mag, and (iv) SN 2006mr suffered no significant host reddening. Although the three methods we have employed for estimating the host reddening are not completely independent — for example, the Lira law has historically been used to calibrate the intrinsic colors of SNe Ia at maximum light (Phillips et al. 1999; Folatelli et al. 2010) — all are consistent in indicating that the four SNe in NGC 1316 were, at most, only slightly reddened.

Maoz & Mannucci (2008) attempted to identify the progenitors of SNe 2006dd and 2006mr using archival *Hubble Space Telescope* (HST) images of NGC 1316. Although they were unable to identify conclusively any point sources, they did estimate the maximum surface brightness attenuation at the position of each SN. Although there are obvious dust features near both SNe (see Figure 1), Maoz & Mannucci (2008) concluded from an analysis based on iso-brightness contours that the maximum surface brightness attenuation at the positions of both SNe was  $A_V^{\text{host}} = 0.25$  mag, which is consistent with the low host reddening values we derive from the SNe light curves. Nevertheless, this method is limited by the resolution of the HST images which, while excellent, may not be sufficient to resolve the smallest dust filaments or holes located in the central regions of NGC 1316.

### 3.3. Distances

#### 3.3.1. SNooPy EBV Method

The distance moduli for SN 1980N, 1981D and 2006dd calculated using the EBV option in SNooPy (see Table 7) are consistent, showing a total variation of only 0.085 mag. Combining the distance estimates into a weighted average must be done with care as there are errors that correlate when averaging over different filters, and errors that correlate when

averaging over different SN.

When computing the error in a weighted average of distances estimated from several SNe, one must consider the errors introduced by different sources including: (1) the statistical errors in the best-fit value of the distance from each SN which depend on the quality of the observations, (2) the intrinsic dispersion in SNe Ia as standard candles, and (3) the uncertainty in the calibration parameters ( $M_X(0)$ ,  $b_X$ ,  $R_X$ ). Some of these errors are highly correlated and this must be taken into account. For instance, an error of  $\delta m$  in  $M_X(0)$  results in the same systematic error  $-\delta m$  in each distance modulus and therefore in the final weighted average. On the other hand, the intrinsic dispersion in SNe Ia is a random error and should diminish as  $1/\sqrt{N}$ . These errors can be propagated analytically by building a correlation matrix, however, we opted to instead use Monte-Carlo simulations. First, the errors listed in Table 9 of Folatelli et al. (2010) and an intrinsic dispersion in SN Ia of 0.06 mag was used to randomly generate 500 realizations of the calibration parameters. We then fit each SN with these realizations, generating 500 distances for each SN. This allowed the systematic error in the distance of each event to be determined, as well as the systematic error in the final weighted average. From this experiment, the systematic error budget for an individual SN is found to be  $\approx \pm 0.07$  (see Table 7), whereas for the weighted average distance modulus this reduces to  $\pm 0.05$ . Note that these values do not include the systematic error in the Hubble constant.

Combining the SNooPy EBV option average distance moduli listed in Table 7, we obtain a final weighted average distance modulus ( $\mu_0 - 5 \log_{10} \cdot h_{72}$ ) of  $31.180 \pm 0.013$  (random)  $\pm 0.050$  (systematic) mag.

### 3.3.2. Tripp Method

As discussed above, SN 2006mr was excluded from the SNooPy analysis because it is a fast-declining [ $\Delta m_{15}(B) = 1.820 \pm 0.020$ ] event that lies outside of the range in which the luminosity–decline rate relations of Folatelli et al. (2010) are applicable. However, these authors have suggested that it may be possible to compute reliable distances from fast-declining SNe Ia using the two-parameter model of Tripp (1998). Following this line of reasoning, we have applied the Tripp method to SN 2006mr, as well as to the three normal events. The Tripp model assumes that the distance modulus of a SN Ia has the following dependence on decline rate and color:

$$\mu_o = m_X^{\max} - M_X(0) - b_X \cdot [\Delta m_{15}(B) - 1.1] - \beta_X^{YZ} \cdot (Y - Z). \quad (7)$$

Here  $m_X^{\max}$  is the observed K-corrected magnitude at maximum corrected for Galactic reddening,  $M_X^0$  is the peak absolute magnitude of SNe Ia with  $\Delta m_{15}(B) = 1.1$  and zero color,  $b_X$  is the slope of the luminosity vs. decline rate relation,  $\beta_X^{YZ}$  is the slope of the luminosity-color relationship, and  $(Y - Z)$  is a pseudo-color at maximum.<sup>12</sup>

To use the Tripp (1998) model to estimate distances requires an accurate calibration between the relations of peak absolute magnitude vs.  $\Delta m_{15}(B)$  and pseudo-colors. These calibrations were obtained using 25 of the 35 *best-observed* SN Ia light curves presented in the first CSP SNe Ia data release (Contreras et al. 2010). The Folatelli et al. (2010) calibration of these relations included SN 2006mr. In order to avoid any circularity we re-computed the relations omitting this SN. The resulting fits of peak absolute magnitude vs.  $\Delta m_{15}(B)$  and pseudo-color for all of the relevant passbands are provided in Table 8. Columns 4–6 give the fit values of  $M_X^0$ ,  $b_X$ , and  $\beta_X^{YZ}$  for each filter and pseudo-color combination. Column 7 gives the values of  $R_V$  implied by the slopes of the luminosity-color relation,  $\beta_X^{YZ}$  assuming the CCM+O reddening law, all of which are consistent with a value of  $R_V^{\text{host}} \sim 1.4$ . With these relations and the measurements of  $m_X^{\max}$  and  $\Delta m_{15}(B)$  given in Table 5, distance moduli were computed for each observed passband.

Considerable care was also taken to compute the systematic uncertainty associated with the Tripp distance estimates. To do so we performed Monte-Carlo simulations in the same way as in § 3.3.1. Taking the K-corrected peak magnitude of each light curve, and the calibration parameters  $M_0$ ,  $b_X$ ,  $\beta_X^{YZ}$  and  $R_X$ , we computed 500 realizations using the errors of these parameters reported in Table 8, and adopted the assumption that only  $M_0$  and  $R_X$  are correlated. From this experiment, we derived a distance modulus for each filter combination and a weighted average using the full correlation matrix from the SNooPy fits. Histograms of the distance moduli were then constructed for each SN and the combined average of the three normal events, from which, the systematic uncertainty was taken as the standard deviation of each distribution.

The results of the Tripp method are given in the penultimate column of Table 7. For SNe 1980N, 1981D, and 2006dd, the derived average distance moduli exhibiting a total range of 0.17 mag. The weighted average distance modulus ( $\mu_0 - 5 \log_{10} \cdot h_{72}$ ) of these three normal events is  $31.248 \pm 0.034$  (random)  $\pm 0.040$  (systematic) mag.

In the case of SN 2006mr, the Tripp method yields an average distance modulus ( $\mu_0 - 5 \log_{10} \cdot h_{72}$ ) of  $31.834 \pm 0.070 \pm 0.080$  mag, which is more than 0.5 mag greater than the weighted average of the three normal events. Contrary to the suggestion of Folatelli et al.

---

<sup>12</sup>A *pseudo-color* is defined to be the difference between peak magnitudes of two passbands. In the case of SNe Ia, the time of peak brightness varies from passband to passband.

(2010) that fast declining SNe Ia follow the Tripp model, the discrepancy in the distance derived here for SN 2006mr compared to the normal objects indicates otherwise. Folatelli et al. (2010) assumed a Surface Brightness Fluctuations (SBF) derived distance modulus to NGC 1316 that is  $\approx 0.3$  mag further than our weighted average, and obtained residuals of  $\sim 0.2$  mag — towards a shorter distance — in all bands with respect to the Tripp fits. These differences account for the  $\sim 0.5$  mag difference obtained here.

### 3.3.3. NIR Method

The NIR light curves of SNe 1980N, 1981D, 2006dd, and 2006mr offer an alternative method for deriving the distance to NGC 1316. Krisciunas, Phillips & Suntzeff (2004) showed that there is little or no dependence on decline rate of the NIR luminosities of SNe Ia, and that these objects are essentially perfect standard candles at these wavelengths. More recently, Krisciunas et al. (2009) have suggested that there may actually be a bimodal distribution of SN Ia luminosities in the NIR in the sense that those that peak in the NIR *prior* to  $T(B)_{\max}$  (like SNe 1980N, 1981D, and 2006dd) have effectively the same NIR absolute magnitudes at maximum light regardless of the value of  $\Delta m_{15}(B)$ , whereas those that peak in the NIR *after*  $T(B)_{\max}$  (like SN 2006mr) are subluminal in all bands.

Table 9 gives the average NIR peak absolute magnitudes,  $M_J$ ,  $M_H$ , and  $M_{K_s}$ , reported in Krisciunas et al. (2009) but modified to exclude SNe 1980N, 1981D and 2006mr. These values can be used with the reddening values listed in Table 6 and the observed peak  $JHK_s$  magnitudes given in Table 5 to derive independent distance moduli for NGC 1316. Combining the distances obtained from the NIR light curves of each SNe, we obtain the distance moduli given in the final column of Table 7. Here the systematic uncertainties were obtained by simply adding the errors of  $M_J$ ,  $M_H$ , and  $M_{K_s}$  in quadrature. This is due to the fact that Krisciunas et al. (2009) calibrated their SNe Ia assuming a fixed value of  $R_V$  and no dependence of the absolute magnitude on  $\Delta m_{15}(B)$ . Therefore, assuming there are no covariances between  $M_J$ ,  $M_H$  and  $M_{K_s}$ , the systematic error is simply the effect of three independent errors. This also applies for the weighted average of the distances derived for the three normal events, for which we find  $\mu_0 - 5.0 \log_{10} \cdot h_{72} = 31.203 \pm 0.012$  (random)  $\pm 0.055$  (systematic) mag.

The NIR distance moduli computed for the normal objects show a larger total range (0.24 mag) than those obtained using either the SNooPy EBV or Tripp methods. This is not surprising since only one of the three, SN 2006dd, was actually observed at maximum in the NIR. The weighted average distance modulus of the three normal SNe is consistent within the quoted uncertainties to the values obtained from the EBV and Tripp methods.



When comparing the NIR-determined distances to those derived with the SNooPy EBV method, one needs to take into account that there is significant covariance between the adopted value of  $R_V$  and the derived  $JHK_s$  absolute magnitudes listed in Table 9. Because the Krisciunas et al. (2009) sample used to derive the values listed in Table 9 has a non-negligible average extinction ( $\langle E(B - V) \rangle = 0.11$ ), changing the assumed value of  $R_V$  from 3.1 to 2.0 will change the calibration in the following way:

$$\Delta M_J = (R_J[R_V = 3.1] - R_J[R_V = 2.0]) \cdot \langle E(B - V) \rangle = 0.05 \text{ mag} \quad (8)$$

$$\Delta M_H = (R_H[R_V = 3.1] - R_H[R_V = 2.0]) \cdot \langle E(B - V) \rangle = 0.03 \text{ mag} \quad (9)$$

$$\Delta M_K = (R_K[R_V = 3.1] - R_K[R_V = 2.0]) \cdot \langle E(B - V) \rangle = 0.02 \text{ mag}. \quad (10)$$

These differences are in the sense that  $\Delta M_X$  should be subtracted from the NIR distance moduli derived using filter  $X$ . While Krisciunas et al. (2009) did not strictly assume  $R_V = 3.1$ , these numbers give a rough idea of the magnitude of the correction.

In the case of the fast-declining SN 2006mr, the NIR distance modulus we derive is  $\sim 0.5$  mag greater than the normal objects. Intriguingly, this is in the same sense and of similar magnitude to the discrepancy found between the distance of SN 2006mr and the three normal SNe derived via the Tripp method.

### 3.3.4. *MLCS2k2*

To ensure that the EBV or Tripp methods, or their adopted calibrations, are not the source of the disagreement between the distances derived from the normal objects and SN 2006mr, the optical light curves of each SN were also fit with MLCS2k2 (Jha, Riess & Kirshner 2007). For this purpose we made use of SN analysis software package *SNANA* (Kessler et al. 2009). Optical light curve fits were performed with photometry in the *standard* Landolt and Smith photometric systems, and  $R_V$  was set to be consistent with the calibration used with the EBV method. From this analysis we find a distance to SN 2006mr that is  $\sim 50\%$  further than the average distance derived from the normal events. This discrepancy is  $\sim 15\%$  worse than what was determined from the EBV and Tripp methods.

#### 4. Na I D Absorption

The spectra of both SNe 2006dd and 2006mr exhibited strong interstellar Na I D absorption lines in the rest system of the host galaxy. The left two panels of Figure 10 show a blow-up of these features in our highest dispersion spectra. The total equivalent widths of the absorption are 3.2 Å for SN 2006dd and 2.4 Å for SN 2006mr, although in both cases the profiles show clear evidence for structure. It is possible to obtain good fits to the profiles assuming that they are composed of two unresolved Na I D doublets. We employed the IRAF<sup>13</sup> “fitprofs” task to deblend the profiles using Gaussian profiles with FWHM values equal to the spectral resolution. The equivalent widths derived from these fits are given in Table 10. According to Munari & Zwitter (1997), the ratio of the D2/D1 equivalent widths is 2.0 in unsaturated lines, and asymptotically approaches a value of 1.1 at high optical depths. The values of this ratio for the two systems in 2006dd are 1.2 and 1.3, while in 2006mr the ratios are 1.2 and 1.1. Hence, we are dealing with saturated lines as expected for such strong absorption.

The right hand panels of Figure 10 show the same spectra of SNe 2006dd and 2006mr in the region of the Ca II H & K lines. Absorption produced by both H & K is clearly present in SN 2006dd. In SN 2006mr, the K line may be weakly present, but the H line is hidden by noise. The total equivalent width of the K line in 2006dd is  $\sim 0.6$  Å; in 2006mr, it is  $\sim 0.2$ – $0.3$  Å. Hence, the Ca II absorption in both SNe is weaker than the Na I D absorption. A Ca II/Na I ratio  $\leq 1$  is typical of lines of sight in the disk of the Milky Way, whereas gas in the halo regions generally shows Ca II/Na I ratio  $\gg 1$  (Cohen & Meloy 1975). The low ratio in the disk gas is generally taken as an indication that there has been significant depletion of Ca in dust grain formation.

According to NED, the radial velocity of NGC 1316 is 1760 km s<sup>−1</sup>. Hence, the interstellar absorption systems observed in *both* SNe are blueshifted with respect to the systemic velocity. Interestingly, the measured velocities of the “B” systems in both SNe are identical to within the errors. The ionized gas in NGC 1316 was shown by Schweizer (1980) to exhibit rapid rotation with the maximum velocity gradient running approximately NW to SE. Relative to the nucleus, the SE side is approaching, and the NW side receding. SNe 2006dd and 2006mr were located to the N and E of the nucleus, respectively. It therefore seems unlikely that simple rotation can explain the observed blueshifts of the interstellar lines in both SNe unless the gas producing the absorption has a different origin than the ionized gas.

---

<sup>13</sup>IRAF is distributed by the National Optical Astronomy Observatory, which is operated by the Association of Universities for Research in Astronomy (AURA) under cooperative agreement with the National Science Foundation.

The brightness of SN 2006dd allowed spectral observations to extend for nearly 7 months. Surprisingly, the strength of the absorption appears to have decreased significantly in the two November 2006 spectra. This is highlighted in the left panel of Figure 11, which displays the evolution of the Na I D spectral region from  $-14$  to  $+191$  days past maximum. In each instance the observed spectrum is over-plotted with the best model determined through Markov chain Monte Carlo (MCMC) fitting simulations.

MCMC is a Bayesian method for determining the posterior probability distribution (PPD) of parameters in a model. It does this by randomly walking through parameter space, creating a Markov chain of states. At each point in the chain, the probability of the state is computed by creating a theoretical realization of the data from the model and noise characteristics we define and comparing this with the actual data. In this way, MCMC is a Monte Carlo simulation. However, because it is also a Markov Chain, in the sense that each state in the chain is probabilistically determined from the previous state, sampling from this chain after it has converged is equivalent to sampling from the PPD. MCMC therefore gives us both the maximum likelihood solution to the problem, as well as a robust estimate of the errors and covariances of the parameters. However, the error estimates depend on the assumed error model of the spectrum. In all cases, we use Poisson noise based on the observed counts and the read noise of the detector. It is possible we are neglecting small sources of error (e.g., extra detector noise) and therefore underestimating the uncertainties in the equivalent widths. This is particularly relevant for our final observation of SN 2006dd, where the signal-to-noise is very low and the significance of the detection, or lack thereof, depends critically on our noise model.

To fit the lines we first modeled the highest resolution, highest signal-to-noise ratio spectrum (21 June 2006) as two systems, i.e. Na I D(A) and Na I D(B) (four Gaussians). The separation of the two doublets was fixed at  $5.97 \text{ \AA}$  while the redshift of each system was allowed to float. From this analysis we computed line ratios of  $1.18 \pm 0.08$  and  $1.36 \pm 0.19$  and total equivalent widths of  $1.24 \pm 0.08 \text{ \AA}$  and  $1.94 \pm 0.08 \text{ \AA}$  for the Na I D(A) and Na I D(B) doublets, and a  $\text{FWHM} = 3.3 \text{ \AA}$ . Note these values are in agreement with what was obtained using the IRAF “fitprofs” task (see Table 10). For the remaining spectra the two Na I doublets are blended together. In this case we imposed priors on all the variables consistent with what was obtained with the 21 June 2006 spectrum, except for the two equivalent width components which were given uniform priors, and the FWHM was set at a constant equal to the resolution of the specific spectrum in question. The total equivalent width values and their associated  $1\text{-}\sigma$  error are provided in each panel on the right of Figure 11. The right panel of Figure 11 shows the PPDs for the total equivalent width for each epoch. To facilitate comparison the PPDs were placed on a single scale so that the differences in equivalent width and the error from the models shown in the left panel

are apparent.

The results of the MCMC fits are summarized in Figure 12 where the total equivalent width of the Na I D absorption (error bars correspond to  $1\sigma$ ) in each spectrum is plotted vs. days past  $B$ -band maximum. The weakening in the line strength of Na I D in the two November spectra is striking. More quantitatively, we find that the equivalent width of the Nov. 16 line differs from the Jun. 21 line at 98% confidence. The Nov. 4 equivalent width differs from the Jun. 21 value at 93% confidence. Taken jointly, the two November equivalent widths differ from the Jun. 21 value at more than 99% confidence.

Contrary to the situation for SN 2006dd, our spectra of SN 2006mr do not show any evidence for a variation in the strength of the Na I D absorption. However, our spectroscopic coverage of SN 2006mr extended to only two months past  $B$  maximum, whereas the apparent weakening of the absorption in SN 2006dd occurred sometime between three and four and a half months after  $B$  maximum.

According to the relation between  $E(B - V)$  and the equivalent width of the Na I D1 line for Galactic stars (Munari & Zwitter 1997), the very strong Na I D absorption observed in SNe 2006dd and SN 2006mr is totally inconsistent with the low host galaxy reddening we derive from the light curve observations. To illustrate the magnitude of this inconsistency, we compare in the upper panel of Figure 13 the  $(B - V)$  color evolution of SN 2006dd with that of two other SNe Ia with similar decline rates: SN 2005na, which was essentially unreddened (Folatelli et al. 2010), and SN 2006X, which exhibited strong Na I D interstellar absorption with an equivalent width of  $\sim 2.0$  Å and a color excess of  $E(B - V) \sim 1.2 - 1.4$  mag (Wang et al. 2008; Folatelli et al. 2010). In the lower panel of the same Figure, the  $(B - V)$  color evolution of SN 2006mr is compared with that of two other fast-declining SNe Ia: SN 1991bg, which appeared in an elliptical galaxy and is assumed to have been unreddened, and SN 1986G, which was heavily obscured [ $E(B - V) \sim 0.7$  mag] by the dust lane in NGC 5128 and showed strong Na I D absorption with an equivalent width of  $\sim 3.6$  Å (Phillips et al. 1987, 1999). As is seen, the color evolution of SNe 2006dd and 2006mr closely resembles that of the two unreddened SNe, yet the strength of the Na I D interstellar absorption was comparable to that observed in the two heavily reddened SNe. Clearly the gas-to-dust ratio in the gas that produced the Na I D absorption in SNe 2006dd and 2006mr is *considerably* different from the typical value in the Milky Way, and also compared to the gas that produced the strong Na I D absorption in SNe 2006X and 1986G.

## 5. Conclusions

The four SNe Ia discovered to date in NGC 1316 provide a unique test of the precision of SN Ia distance determinations. Employing three different methods, we find excellent agreement between the three “normal” SNe, 1980N, 1981D, and 2006dd for each technique. The standard deviations of the distance moduli for the three SNe using the SNOoPy EBV option, the Tripp method, and NIR light curves are 4%, 8%, and 10%, respectively. Moreover, the agreement between the average distance moduli obtained with each technique is exceptional (better than 3%). On the basis of these results, it would appear that distances to SNe Ia can be measured to better than 5% using present methods. This finding supports the recent conclusion of Folatelli et al. (2010) that it is possible to measure SN Ia distances to a relative precision of 3-4%, as well as the work of Riess et al. (2009), who found a relative dispersion of 4% between SNe Ia distances and Cepheid distances to the host galaxies of these same SNe.

Our attempts to derive a distance to NGC 1316 based on the fast-declining event SN 2006mr were less successful. Using the two-parameter (Tripp) method gives a distance modulus which is  $\sim 0.5$  mag larger (or 25 – 30% further in distance) than the values derived for the three “normal” SNe Ia using the same method. The distance modulus derived for SN 2006mr from the NIR light curves is also  $\sim 0.5$  mag larger than that obtained for the three normal SNe, even when we use the bimodal distribution of absolute magnitudes in the NIR recently proposed by Krisciunas et al. (2009). Clearly more optical and NIR observations of fast-declining SNe Ia are necessary in order to definitively answer the question of whether these events can be used to determine precise distances.

Based on the three “normal” SNe Ia in NGC 1316, our best estimate for the distance modulus of this galaxy is  $(\mu_0 - 5 \log_{10} \cdot h_{72}) = 31.248 \pm 0.034$  (random)  $\pm 0.040$  mag (systematic) or  $17.8 \pm 0.3$  (random)  $\pm 0.3$  (systematic) Mpc for  $H_o = 72$ . Here, we have adopted the distances derived using the Tripp method as representative of the three methods employed. This value is in excellent accord with the Planetary Nebula Luminosity Function (PNLF) distance modulus of  $\mu = 31.26^{+0.09}_{-0.12}$  mag derived by Feldmeier, Jacoby, & Phillips (2007). Somewhat worse agreement is found with the SBF measurements of  $\mu = 31.59 \pm 0.08$  mag by Cantiello et al. (2007) and  $\mu = 31.606 \pm 0.065$  mag by Blakeslee et al. (2009). We note that our SN Ia distance modulus for NGC 1316 is  $\sim 0.4$  mag closer than the value quoted by Goudfrooij et al. (2001), and for which no details were given. These authors argued that the SN distance placed NGC 1316  $\sim 0.25$  mag behind the core of the Fornax cluster. However, our SN Ia distance, as well as the PNLf and SBF determinations imply that NGC 1316 is very nearly at the same distance as the cluster core, which SBF observations place at  $\mu = 31.51 \pm 0.03$  mag (Blakeslee et al. 2009). A further check is provided by SN 1992A,

which appeared in the Fornax cluster member NGC 1380. From photometry presented by Suntzeff (1996), we derive a distance modulus of  $\mu = 31.611 \pm 0.008$  mag using SNOOpy and the absolute magnitude–decline rate calibrations given by Prieto et al. (2006). The PNLf distance to NGC 1380 is  $\mu = 31.04^{+0.11}_{-0.12}$  mag, which prompted Feldmeier, Jacoby, & Phillips (2007) to speculate that SN 1992A was  $\sim 0.4$  mag underluminous. However, the most recent SBF determination of  $\mu = 31.632 \pm 0.075$  mag (Blakeslee et al. 2009) is in comfortable agreement with the SN Ia determination.

The host galaxy reddening values derived from the light curve observations for all four SNe in NGC 1316 are modest or negligible. Nevertheless, spectra of the two innermost events, 2006dd and 2006mr, show strong Na I D interstellar absorption lines at the redshift of NGC 1316. Such prominent absorption is *always* accompanied by strong dust reddening in the interstellar medium of our own Galaxy (Munari & Zwitter 1997). The implication is that the gas-to-dust ratio in the central regions of NGC 1316 is unusually large. Although a plausible explanation for this might be that the dust has been destroyed by UV emission produced from the relatively recent star formation in NGC 1316 (Schweizer 1980; Goudfrooij et al. 2001), the HST images published by Maoz & Mannucci (2008) undeniably reveal the existence of significant dust near the positions of both SNe.

If the gas producing the Na I absorption were to lie inside the dust evaporation radius of  $\sim 10^{17}$  cm (Chugai 2008), then the high gas-to-dust ratio could be due to the supernova explosion itself. The weakening of the Na I absorption at  $\sim 105$  days after explosion could, in turn, be due to the SN ejecta overtaking the cloud producing the absorption. If we assume a maximum velocity of the ejecta of  $\sim 3 \times 10^9$  cm s $^{-1}$ , then a distance of the gas from the SN of  $\sim 3 \times 10^{16}$  cm ( $\sim 0.01$  pc) is implied. Nevertheless, the flux of a SN Ia is sufficient to ionize gas out to  $\sim 5 \times 10^{18}$  cm (Patat et al. 2007), so the sodium in such a cloud would be ionized at outburst. The fact that we observe a constant equivalent width of the Na I D lines from -11.5 to +86.4 days with respect to  $B$  maximum requires that the Na recombine within a week of explosion. Even if the gas is in the form of dense ( $\sim 10^7$  cm $^{-3}$ ) filaments, a gas cloud lying at a distance of 0.01 pc from the SN would not have recombined before our first spectroscopic observation (Simon et al. 2009). Indeed, a distance of at least  $\sim 10$  pc is implied. The apparent recovery of the Na I absorption  $\sim 170$  days after explosion also appears to be inconsistent with this scenario although, as mentioned previously, the reality of the detection of the Na I absorption in our last spectra depends considerably on the assumed signal-to-noise of the spectrum.

Alternatively, the variation of the Na I absorption could be due to the changing angular size of the SN as it expands (Chugai 2008). According to Patat et al. (2010), the maximum radius of a SN Ia in the photospheric phase ( $t < 100$  days) is  $\sim 10^{17}$  cm. At the end of

the photospheric phase, the effective radius of the SN should decrease rapidly as the ejecta become optically thin. Moreover, the Na I absorption happens to lie near the peak of a [Co III] emission feature which was decaying rapidly over the  $\sim 25$  day interval when the strong decrease in the Na I absorption was observed. It is unclear whether this scenario can account for the possible increase in the Na I absorption seen in our final spectra, and does not explain the high gas-to-dust ratio.

SNe 2006dd and SN 2006mr are not the only apparently low-reddened SNe Ia to display strong Na I D interstellar absorption lines. Figure 10 of Folatelli et al. (2010) indicates that the normal  $[\Delta m_{15}(B) = 1.02]$  SN 2005bg had a Na I D equivalent width of  $\sim 2.0$  Å; see also Figure 5 of Blondin et al. (2009) which contains several objects with relatively strong Na I D absorption accompanied with low to modest host reddening. Nevertheless, the reddening for this SN, as estimated from both the colors at maximum light and the Lira Law, is negligible. Absorption in the Ca II H & K lines was also visible in SN 2005bg, with the ratio of the Ca II/Na I equivalent widths  $\sim 1$ . Unfortunately, spectroscopic observations of SN 2005bg were obtained only for a few days around maximum light, so it is not possible to look for variations of the Na I D equivalent width. Indeed, very few SNe Ia have been observed with signal-to-noise ratio large enough to be able to detect a variation like that observed in SN 2006dd.

The glaring inconsistency between the presence of strong interstellar line absorption, yet the absence of evidence for significant dust reddening highlights our current ignorance of the host galaxy reddening properties of SNe Ia. On the one hand, we have shown in this paper that application of three different methods for determining distances to SNe Ia gives results that are stunningly consistent for the three normal SNe Ia in NGC 1316, and which support recent evidence that these objects can be used to measure cosmological distances to a precision of  $< 5\%$ . On the other hand, we are at a loss to explain how two of the SNe in NGC 1316 could show such strong interstellar Na I D lines when the same methods used to determine such precise distances indicate that both SNe suffered small or negligible host galaxy reddening. The treatment of dust extinction in SNe Ia is considered by many (e.g., see Wood-Vasey et al. 2007) to be the single largest source of systematic error in using these objects to constrain the dark energy equation of state in next-generation experiments. While the SNe in NGC 1316 confirm that SNe Ia are potentially one of the most powerful tools for studying cosmology, they also remind us that there is still much left to understand regarding the properties of these explosions and their progenitor systems.

We owe a debt of gratitude to Rick Kessler for performing the MLCS2k2 fits discussed in § 3.3.4. We are grateful to D. Watson, J. Prieto, P. Höflich, J. Sollerman and J. Fynbo for stimulating discussions related to this work. We acknowledge the Aspen Center for Physics

for hosting the summer meeting “Taking Supernova Cosmology into the Next Decade”, during which this paper was being finalized and benefitted from discussions with other participants. A special thanks to J. Prieto, D. DePoy, L. Watson, C. Morgan and M. Eyler for the 05 Nov. 2006 spectrum of SN 2006dd, and the 20 Nov. 2006 spectrum of SN 2006mr. This material is based upon work supported by the National Science Foundation (NSF) under grant AST–0306969. The Dark Cosmology Centre is funded by the Danish NSF. GF and MH acknowledges support from Iniciativa Científica Milenio through grant P06-045-F and CONICYT through Centro de Astrofísica FONDAP (grant 15010003), Programa Financiamiento Basal (grant PFB 06), and Fondecyt (grant 1060808 and 3090004). The CTIO 1.3-m telescope is operated by the Small and Moderate Aperture Research Telescope System (SMARTS) Consortium. We have made use of the NASA/IPAC Extragalactic Database (NED) which is operated by the Jet Propulsion Laboratory, California Institute of Technology, under contract with the National Aeronautics and Space Administration. This publication makes use of data products from the Two Micron All Sky Survey, which is a joint project of the University of Massachusetts and the Infrared Processing and Analysis Center/California Institute of Technology, funded by the National Aeronautics and Space Administration and the National Science Foundation.

## REFERENCES

- Blakeslee, J. P., et al. 2009, *ApJ*, 694, 556
- Blanco, V., et al. 1980, *IAUC*, 3556
- Blondin, S., et al., *ApJ*, 2009, 693, 207
- Burns, C., et al. 2010, *AJ*, submitted
- Cantiello, M., et al. 2007, *ApJ*, 668, 130
- Cardelli, J. A., Clayton, G. C., & Mathis, J. S. 1989, *ApJ*, 345, 245
- Chugai, N. N. 2008, *AstL*, 34, 389
- Cohen, J. G., & Meloy, D. A. 1975, *ApJ*, 198, 545
- Contreras, C., Hamuy, M., Phillips, M. M., et al. 2010, *AJ*, 139, 519
- Cragg, T., Evans, R., & Maza, J. 1981, *IAUC*, 3583
- Draine, B. T., et al. 2007, *ApJ*, 663, 866



- Elias, J. H., Frogel, J. A., Hackwell, J. A. Persson, S. E. 1981, ApJ, 251, L13
- Elias, J. H., Frogel, J. A., Matthews, K., & Neugebauer, G. 1982, AJ, 87, 1029
- Evans, R., & Maclean, N. S. W. 1982, IAUC, 3697
- Feldmeier, J. J., Jacoby, G. H., & Phillips, M. M. 2007, ApJ, 657, 76
- Filippenko, A., Richmond, M., Branch, D., et al. 1992, AJ, 104, 1543
- Folatelli, G., et al. 2010, AJ, 139, 120
- Freedman, W. L., et al. 2009, ApJ, 704, 1036
- Garnavich, P., et al. 2004, ApJ, 613, 1120
- Geldzahler, B. J., & Fomalong, E., B. 1984, AJ, 89, 1650
- Goudfrooij, P., et al. 2001, MNRAS, 322, 643
- Hamuy, M., et al. 1991, AJ, 102, 208
- Hamuy, M., et al. 2006, PASP, 118, 2
- Hao, H., et al. 2007, ApJ, 659, L99
- Hsiao, E., et al. 2007, ApJ, 663, 1187
- Hsiao, E., et al. 2010, in preparation
- Jha, S., Riess, A. G., & Kirshner, R. P. 2007, ApJ, 659, 122
- Kessler, R., et al. 2009, PASP, 121, 1028
- Krisciunas, K., et al. 2000, ApJ, 539, 658
- Krisciunas, K., et al. 2003, AJ, 125, 166
- Krisciunas, K., Phillips, M. M., & Suntzeff, N. B. 2004, ApJ, 602, L84
- Krisciunas, K., et al. 2006, AJ, 131, 1639
- Krisciunas, K., et al. 2007, AJ, 133, 58
- Krisciunas, K., et al. 2009, AJ, 138, 1584
- Lair, J., C., et al. 2006, AJ, 132, 2024

- Landolt, A. 1992, *AJ*, 104, 340
- Leibundgut, B., et al. 1993, *AJ*, 105, 301
- Leibundgut, B. 2008, *General Relativity and Gravitation*, 40, 221
- Lira, P. 2005, Masters Thesis, University of Chile
- Maoz, D., & Mannucci, F. 2008, *MNRAS*, 388, 421
- Maza, J., & Wischnjewsky, M. 1980, *IAUC*, 3548
- Menzies, J. W. 1981, *IAUC*, 3589
- Monard, L. A. G. 2006, *CBET*, 553
- Monard, L. A. G. 2006, *CBET*, 723
- Morrell, N., Folatelli, G., Barba, R., Arias, J. 2006, *CBET*, 564
- Munari, U., & Zwitter, T. 1997, *A&A*, 318, 269
- Nowak, N., et al. 2008, *MNRAS*, 391, 1629
- ODonnell, J. E. 1994, *ApJ*, 422, 158
- Olszewski, E. W. 1982, *I.B.V.S.* No. 2065
- Patat, F., et al. 2007, *Science*, 317, 924
- Patat, F., Cox, N. L. J., Parrent, J., & Branch, D. 2010, *A&A*, 514, 78
- Persson, S. E., et al. 1998, *AJ*, 116, 2475
- Phillips, M. M., et al. 1987, *PASP*, 99, 592
- Phillips, M. M. 1993, *ApJ*, 413, L105
- Phillips, M. M., et al. 1999, 118, 1766
- Phillips, M. M., Folatelli, G., Contreras, C., Morrell, N. 2006, *CBET*, 728
- Prabhu, T. P. 1981, *BASIn*, 9, 60
- Prieto, J. L., Rest, A., & Suntzeff, N. B. 2006, *ApJ*, 647, 501
- Riess, A. G., et al. 2009, *ApJ*, 699, 539

- Salvo, M., Blackman, J., Schmidt, B., Bessell, M. 2006, CBET, 557
- Schlegel, D. J., Finkbeiner, D. P., & Davis, M. 1998, ApJ, 500, 525
- Schweizer, F. 1980, ApJ, 237, 303
- Simon, J. D., et al. 2009, ApJ, 702, 1157
- Smith, J. A., et al. 2002, AJ, 123, 2121
- Stritzinger, M., Hamuy, M., Suntzeff, N. B., et al. 2002, AJ, 124, 2100
- Sullivan, M., et al. 2010, MNRAS, in press (arXiv:1003.5119)
- Suntzeff, N. B. 1996, in IAU Colloq. 145: Supernovae and Supernova Remnants, 41
- Suntzeff, N. B. 2000, in Cosmic Explosions, ed. S. S. Holt & W. W. Zhang (New york: AIP), 65
- Taubenberger, S., et al. 2008, MNRAS, 385, 75
- Tripp, R. 1998, A&A, 331, 815
- Turrato, M., et al. 1996, MNRAS, 283, 1
- Tsvetkov, D., & Bartunov, O. S. 1993, Bull. Inf. Centre Donnees Stellaires, 42, 17
- Walker, W. S. G., & Marino, B. F. 1982, Publ. Var. Star Sect. RASNZ, 10, 53
- Wang, X., et al. 2008, ApJ, 675, 626
- Wang, X., et al. 2009, ApJ, 699, L139
- Wood-Vasey, W. M., et al. 2007, ApJ, 666, 694

Table 1. Spectroscopic observations

Date	Julian Date JD−2,453,000	Epoch <sup>a</sup> (days)	Telescope	Instrument	Range (Å)	Resolution (FWHM Å)	Ncombine	Integration (sec)
<b>2006dd</b>								
2006 June 21	907.9	−11.5	Baade	IMACS	3410 – 9610	3.3	2	600
2006 Sept. 27	1005.8	+86.4	Du Pont	WFCCD	3800 – 9235	8.0	3	600
2006 Nov. 5	1046.5	+125.5	Hiltner	B&C	3868 – 7320	14	4	600
2006 Nov. 16	1055.7	+136.8	Du Pont	WFCCD	3800 – 9235	8.0	3	600
2007 Jan. 6	1106.8	+187.4	NTT	EMMI	3500 – 9610	8.0	3	200
2007 Jan. 13	1113.8	+194.4	Du Pont	B&C	3905 – 10000	8.0	3	900
<b>2006mr</b>								
2006 Nov. 9	1048.8	−2.1	Clay	LDSS	3800 – 9975	2.4	2	120
2006 Nov. 13	1052.8	+1.9	Baade	IMACS	4260 – 9510	3.6	2	150
2006 Nov. 16	1055.7	+4.9	Du Pont	WFCCD	3800 – 9235	8.0	3	300
2006 Nov. 19	1058.5	+7.6	Du Pont	WFCCD	3800 – 9235	8.0	3	300
2006 Nov. 20	1059.5	+8.5	Hiltner	B&C	3835 – 7289	14	3	300
2006 Nov. 22	1061.8	+10.8	Du Pont	WFCCD	3800 – 9235	8.0	3	300
2006 Dec. 18	1087.8	+36.8	Du Pont	WFCCD	3860 – 9235	8.0	3	500
2007 Jan. 13	1113.8	+62.9	Du Pont	B&C	3905 – 10000	8.0	3	600

<sup>a</sup>Days since  $T(B)_{\max}$ .

Table 2. Photometry of the CTIO Local Sequence in the Standard System

ID	R.A.	Decl.	<i>B</i>	<i>V</i>	<i>R</i>	<i>I</i>	<i>J</i>	<i>H</i>	<i>K<sub>s</sub></i>
CSP02	3 <sup>h</sup> 22 <sup>m</sup> 38 <sup>s</sup> .36	−37°14′45″.31	16.180(005)	15.567(007)	15.203(008)	14.858(008)	12.807(006)	12.213(007)	12.077(012)
CSP03	3 <sup>h</sup> 22 <sup>m</sup> 31 <sup>s</sup> .62	−37°13′51″.46	16.812(008)	15.682(004)	14.996(004)	14.412(008)	...	...	...
CSP06	3 <sup>h</sup> 22 <sup>m</sup> 34 <sup>s</sup> .23	−37°10′01″.71	17.470(008)	16.859(006)	16.489(007)	16.114(006)	...	...	...
CSP50	3 <sup>h</sup> 22 <sup>m</sup> 44 <sup>s</sup> .55	−37°12′46″.94	16.204(011)	15.027(005)	14.288(007)	13.684(008)	...	...	...

Note. — Uncertainties given in parentheses in millimag.

Table 3. Optical and Near-IR Photometry of SN 2006dd in the natural system of the CTIO 1.3-m telescope

JD–2, 453, 000	Phase <sup>a</sup>	<i>B</i>	<i>V</i>	<i>R</i>	<i>I</i>	<i>J</i>	<i>H</i>	<i>K<sub>s</sub></i>
908.90	–10.5	13.579(009)	13.629(007)	13.423(008)	13.398(011)	13.477(021)	13.537(024)	13.692(034)
912.91	–6.5	12.713(008)	12.788(007)	12.612(008)	12.642(010)	12.851(013)	...	12.853(020)
914.90	–4.5	12.498(009)	12.588(009)	12.437(008)	12.499(009)	12.755(019)	12.843(019)	12.784(026)
918.90	–0.5	12.336(009)	12.380(008)	12.290(013)	12.516(011)	12.825(021)	12.850(025)	12.714(028)
930.88	+11.5	13.033(017)	12.733(009)	12.755(011)	13.103(013)	14.346(037)	13.393(025)	13.259(023)
933.88	+14.5	13.347(009)	12.948(008)	12.902(009)	13.161(010)	14.444(029)	13.296(022)	13.290(023)
937.86	+18.5	...	...	...	...	14.456(029)	13.063(021)	12.974(021)
941.89	+22.5	...	...	...	...	14.139(026)	12.909(020)	12.858(020)
945.88	+26.5	14.682(011)	13.643(009)	13.167(010)	12.936(011)	13.821(023)	12.856(019)	12.823(020)
951.86	+32.5	15.106(015)	14.039(014)	13.559(012)	13.241(023)	13.878(034)	13.133(025)	13.082(025)
961.79	+42.4	15.430(011)	14.465(008)	14.064(013)	13.827(011)	14.725(031)	13.687(025)	13.660(023)
968.83	+49.5	15.547(013)	14.663(011)	14.308(016)	14.128(019)	15.323(040)	14.024(027)	14.066(022)
974.82	+55.4	15.634(011)	14.816(011)	14.518(013)	14.400(018)	15.607(046)	14.233(031)	14.253(023)
980.84	+61.4	...	...	...	...	16.081(021) <sup>b</sup>	14.606(020) <sup>b</sup>	...
993.82	+74.3	...	...	...	...	16.798(043) <sup>b</sup>	.....	...
995.85	+76.4	...	...	...	...	16.931(035) <sup>b</sup>	15.267(020) <sup>b</sup>	...

Note. — Uncertainties given in parentheses in millimag and include the usual photon statistics as well as errors in the zero points.

<sup>a</sup>Days since  $T(B)_{\max}$ .

<sup>b</sup>Photometry obtained with the Swope telescope equipped with RetroCam. This photometry is in the natural system of the Swope telescope.

Table 4. Optical Photometry of SN 2006dd in the natural system of the Swope telescope

JD–2, 453, 000	Phase <sup>a</sup>	<i>u</i>	<i>g</i>	<i>r</i>	<i>i</i>	<i>B</i>	<i>V</i>
979.92	+60.534	...	15.286(004)	14.804(004)	...	...	...
981.84	+62.451	16.893(019)	15.301(006)	14.829(009)	15.041(009)	15.691(007)	14.903(007)
986.84	+67.452	16.997(021)	15.391(005)	15.025(004)	15.236(006)	15.784(007)	15.047(006)
994.85	+75.462	17.154(019)	15.521(004)	15.265(006)	15.514(008)	15.892(006)	15.232(006)
998.86	+79.469	17.263(021)	15.585(006)	15.393(007)	15.654(009)	15.958(007)	15.326(007)
1001.90	+82.509	17.308(022)	15.632(009)	15.488(011)	15.736(016)	16.017(008)	15.407(007)
1007.91	+88.518	...	...	...	...	16.102(010)	15.553(006)
1014.82	+95.435	17.606(027)	15.858(011)	15.916(015)	16.173(013)	16.199(007)	15.717(006)
1017.83	+98.438	17.712(031)	15.900(008)	16.013(009)	16.277(012)	16.265(011)	15.786(012)
1046.68	+127.28	18.429(038)	16.373(006)	16.863(009)	17.040(013)	16.731(009)	16.394(009)
1048.82	+129.42	18.553(043)	16.415(006)	16.910(010)	17.105(015)	16.750(009)	16.436(008)
1049.78	+130.39	18.518(035)	16.432(015)	16.936(023)	17.112(022)	16.777(014)	16.439(013)
1052.75	+133.36	18.494(032)	16.504(015)	17.024(026)	17.181(027)	16.817(013)	16.515(016)
1056.74	+137.35	18.658(037)	16.548(009)	17.142(018)	17.282(023)	16.898(011)	16.578(013)
1060.78	+141.38	18.677(045)	16.622(016)	17.245(024)	17.371(033)	16.944(014)	16.680(018)
1065.76	+146.37	18.828(043)	16.713(013)	17.373(019)	17.447(028)	17.024(014)	16.769(018)
1066.83	+147.44	18.853(035)	16.709(011)	17.384(019)	17.515(026)	17.034(014)	16.777(014)
1068.76	+149.37	18.906(038)	16.740(010)	17.462(022)	17.517(028)	17.066(015)	16.796(016)
1071.67	+152.27	18.924(051)	16.789(011)	17.547(018)	17.597(033)	17.155(013)	16.891(014)
1073.73	+154.33	18.947(059)	16.822(009)	17.577(016)	17.605(023)	17.161(011)	16.908(012)
1076.72	+157.33	19.079(073)	16.868(009)	17.663(018)	17.667(027)	17.224(012)	16.969(012)
1080.78	+161.38	19.170(059)	16.938(009)	17.729(023)	17.730(032)	17.279(012)	17.031(011)
1084.68	+165.29	19.252(042)	16.994(009)	17.824(023)	17.812(022)	17.345(012)	17.100(012)
1087.63	+168.24	19.300(044)	16.983(015)	17.867(030)	17.830(032)	17.395(012)	17.073(018)
1092.68	+173.29	19.475(045)	17.050(013)	17.989(031)	17.955(031)	17.483(014)	17.199(016)
1096.66	+177.27	19.521(052)	17.141(009)	18.099(023)	18.012(029)	17.537(011)	17.262(012)
1099.63	+180.24	19.520(075)	17.232(009)	18.183(020)	18.063(029)	17.567(010)	17.359(012)
1100.65	+181.26	19.889(086)	17.259(008)	18.210(022)	18.107(028)	17.605(011)	17.352(013)
1104.72	+185.33	...	17.298(012)	18.257(025)	18.104(034)	17.682(018)	17.442(016)
1106.65	+187.26	...	17.333(008)	18.338(025)	18.146(033)	17.700(012)	17.472(014)
1108.65	+189.26	...	17.303(014)	18.378(032)	18.167(042)	17.731(013)	17.460(017)
1110.61	+191.22	...	17.416(015)	18.380(049)	18.152(045)	17.773(019)	17.548(021)
1118.67	+199.28	...	17.515(009)	18.568(038)	18.351(055)	...	...
1123.63	+204.24	...	17.585(010)	18.762(040)	18.471(051)	17.943(016)	17.750(017)
1127.69	+208.29	...	17.646(011)	18.768(056)	...	17.988(015)	17.812(015)
1130.57	+211.17	...	17.712(013)	18.917(041)	18.529(044)	18.069(041)	17.835(017)
1133.60	+214.21	...	17.727(012)	18.898(038)	18.492(040)	18.112(016)	17.902(017)
1136.63	+217.23	...	17.773(010)	19.016(046)	18.559(051)	18.124(025)	17.954(019)
1143.56	+224.17	...	17.863(016)	19.117(051)	18.686(051)	18.263(018)	17.995(022)
1147.57	+228.17	...	17.957(013)	19.151(056)	18.753(064)	18.342(017)	18.125(020)

Note. — Uncertainties given in parentheses in millimag and include the usual photon statistics as well as errors in the zero points.

<sup>a</sup>Days since  $T(B)_{\max}$ .

Table 5. Maximum Light Magnitudes of SNe 1980N, 1981D, 2006dd & 2006mr

SN	$T(B)_{\max}$ JD-2,400,000	$\Delta m_{15}(B)^a$	$B$	$V$	$r$	$i$	$J$	$H$	$K_s$
1980N	44584.36 $\pm$ 0.24	1.105 $\pm$ 0.019	12.375 $\pm$ 0.016	12.306 $\pm$ 0.016	12.361 $\pm$ 0.027	12.952 $\pm$ 0.035	12.679 $\pm$ 0.062	13.035 $\pm$ 0.042	13.047 $\pm$ 0.102
1981D	44679.51 $\pm$ 0.30	1.212 $\pm$ 0.050	12.600 $\pm$ 0.051	12.381 $\pm$ 0.025	...	...	12.886 $\pm$ 0.055	13.047 $\pm$ 0.029	13.252 $\pm$ 0.049
2006dd	53919.41 $\pm$ 0.08	1.080 $\pm$ 0.014	12.238 $\pm$ 0.009	12.311 $\pm$ 0.009	12.310 $\pm$ 0.011	12.832 $\pm$ 0.010	12.731 $\pm$ 0.014	12.839 $\pm$ 0.020	12.807 $\pm$ 0.060
2006mr	54050.94 $\pm$ 0.12	1.820 $\pm$ 0.020	15.402 $\pm$ 0.014	14.612 $\pm$ 0.010	14.378 $\pm$ 0.014	14.503 $\pm$ 0.009	14.056 $\pm$ 0.007	13.850 $\pm$ 0.006	...

<sup>a</sup>Derived from SNooPy “max” fits or in the case of SN 2006mr via spline fits.

Note. — Peak magnitudes estimated from photometry K-corrected and corrected for Galactic reddening.



Table 6. Host Galaxy Reddenings of SNe Ia in NGC 1316

SN	SNooPy EBV	$E(B - V)_{\text{Host}}$	
		Lira Law	$V - \text{NIR}$
1980N	$0.060 \pm 0.011$	$0.081 \pm 0.027$	$-0.021 \pm 0.010$
1981D	$0.078 \pm 0.024$	...	$-0.025 \pm 0.015$
2006dd	$0.043 \pm 0.008$	$-0.013 \pm 0.005$	$0.093 \pm 0.038$
2006mr	...	$-0.025 \pm 0.013$	...

Table 7. Distances of SNe Ia in NGC 1316

SN	$\Delta m_{15}(B)^a$	$\mu_0^b$ SNooPy EBV	$\mu_0^b$ Tripp	$\mu_0^c$ NIR
1980N	$1.105 \pm 0.011$	$31.211 \pm 0.028 \pm 0.065$	$31.264 \pm 0.055 \pm 0.060$	$31.238 \pm 0.034 \pm 0.055$
1981D	$1.212 \pm 0.071$	$31.242 \pm 0.036 \pm 0.081$	$31.103 \pm 0.090 \pm 0.080$	$31.398 \pm 0.033 \pm 0.055$
2006dd	$1.078 \pm 0.025$	$31.157 \pm 0.016 \pm 0.068$	$31.276 \pm 0.048 \pm 0.070$	$31.162 \pm 0.014 \pm 0.055$
combined	...	$31.180 \pm 0.013 \pm 0.050$	$31.248 \pm 0.034 \pm 0.040$	$31.203 \pm 0.012 \pm 0.055$
2006mr	$1.820 \pm 0.020$	...	$31.834 \pm 0.070 \pm 0.080$	$31.739 \pm 0.005 \pm 0.052$

<sup>a</sup>Derived from SNooPy EBV fits or in the case of SN 2006mr via spline fit.

<sup>b</sup>Uncertainties correspond to fit and systematic errors. The systematic errors were computed from Monte-Carlo simulations (see § 3.3). Also note these errors do not include the uncertainty associated with the Hubble constant.

<sup>c</sup>Uncertainties correspond to fit, reddening and systematic errors (see text).

Table 8. Fits of peak magnitudes versus  $\Delta m_{15}(B)$  and pseudocolor

Fit No.	Filter $X$	Pseudocolor $(Y - Z)$	$M_X(1.1, 0)$	$b_X$	$\beta_X^{YZ}$	$R_V$ (CCM+O)	$\sigma_{\text{SN}}$ [mag]	RMS [mag]	$N_{\text{SNe}}$
(1)	(2)	(3)	(4)	(5)	(6)	(7)	(8)	(9)	(10)
1	$B$	$(B - V)$	$-19.09 \pm 0.02$	$0.70 \pm 0.10$	$2.70 \pm 0.11$	$1.42 \pm 0.10$	0.11	0.15	25
2	$V$	$(B - V)$	$-19.09 \pm 0.02$	$0.70 \pm 0.10$	$1.70 \pm 0.11$	$1.42 \pm 0.10$	0.11	0.15	25
3	$u$	$(u - V)$	$-19.35 \pm 0.03$	$0.52 \pm 0.10$	$1.73 \pm 0.04$	$1.08 \pm 0.07$	0.09	0.13	24
4	$g$	$(g - r)$	$-18.85 \pm 0.01$	$0.84 \pm 0.10$	$2.24 \pm 0.11$	$1.52 \pm 0.12$	0.12	0.15	25
5	$r$	$(B - r)$	$-18.94 \pm 0.01$	$0.81 \pm 0.11$	$0.90 \pm 0.08$	$1.46 \pm 0.11$	0.12	0.15	25
6	$i$	$(B - V)$	$-18.49 \pm 0.02$	$0.56 \pm 0.11$	$1.05 \pm 0.11$	$1.68 \pm 0.12$	0.12	0.15	25
7	$Y$	$(B - V)$	$-18.45 \pm 0.01$	$0.39 \pm 0.12$	$0.55 \pm 0.11$	$1.80 \pm 0.17$	0.10	0.15	19
8	$J$	$(V - J)$	$-18.34 \pm 0.03$	$0.57 \pm 0.08$	$0.17 \pm 0.06$	$1.45 \pm 0.25$	0.04	0.13	20
9	$H$	$(V - H)$	$-18.21 \pm 0.04$	$0.28 \pm 0.15$	$0.20 \pm 0.08$	$2.75 \pm 1.74$	0.12	0.15	18
10	$K$	$(V - K)$	$-18.34 \pm 0.04$	$0.79 \pm 0.29$	$0.15 \pm 0.10$	$4.15 \pm 8.48$	0.10	0.17	9

Note. — Fits of the type:  $\mu_X = m_X^{\text{max}} - M_X(1.1, 0) - b_X [\Delta m_{15}(B) - 1.1] - \beta_X^{YZ} (Y - Z)$ .  
Columns: (1) Fit identifier; (2) Filter corresponding to  $m_X^{\text{max}}$ ; (3) Color; (4) Absolute magnitude for  $\Delta m_{15}(B) = 1.1$  and zero  $(Y - Z)$  color; (5) Luminosity-decline rate slope; (6) Luminosity-color slope; (7) Corresponding parameter  $R_V$  of the CCM+O reddening law; (8) Resulting intrinsic dispersion of SN data; (9) RMS of fit in magnitudes; (10) Number of SNe used in fit.

Table 9. Near-IR absolute magnitudes at maximum<sup>a</sup>

Group	Filter	$\langle M \rangle$	N
Peak early:			
	$J$	$-18.611 \pm 0.033$	23
	$H$	$-18.318 \pm 0.029$	23
	$K$	$-18.442 \pm 0.033$	21
Peak late:			
	$J$	$-17.847 \pm 0.050$	4
	$H$	$-17.895 \pm 0.013$	4

<sup>a</sup>Normal SNe Ia typically peak in the near-IR 3 days before  $T(B)_{\max}$ . SNe Ia that peak in the near-IR a few days after  $T(B)_{\max}$  are fast decliners at optical wavelengths and are faint in all bands.

Table 10. Equivalent Widths and Velocities of Na I D Lines

System	Heliocentric	Equivalent Width (Å)	
	Velocity (km s <sup>-1</sup> )	D1	D2
2006dd			
A	1380 ± 15	0.62 ± 0.04	0.73 ± 0.03
B	1587 ± 15	0.89 ± 0.04	0.98 ± 0.05
2006mr			
A	1466 ± 12	0.44 ± 0.03	0.51 ± 0.02
B	1585 ± 12	0.81 ± 0.03	0.62 ± 0.03

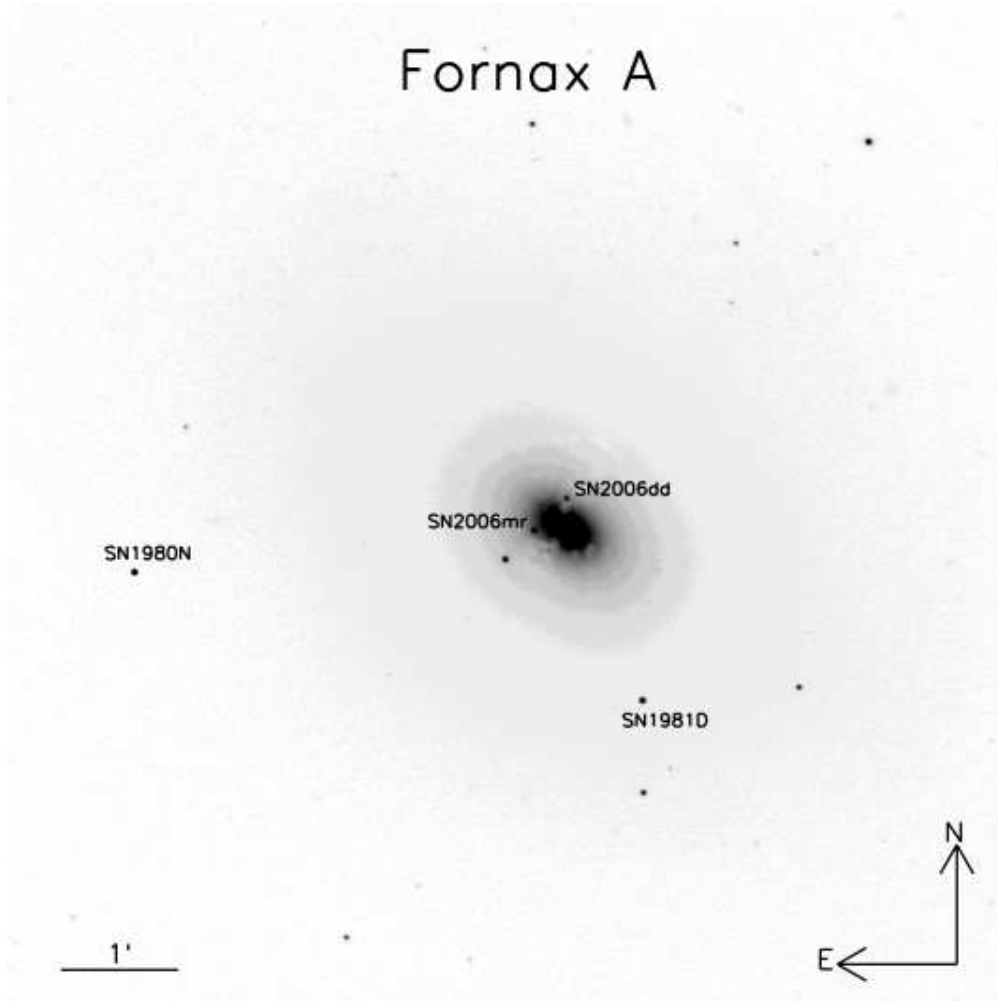


Fig. 1.— A Swope 1 m telescope *V*-band image of NGC 1316 obtained in 2006. Artificial stars have been placed at the coordinates of SN 1980N and SN 1981D.

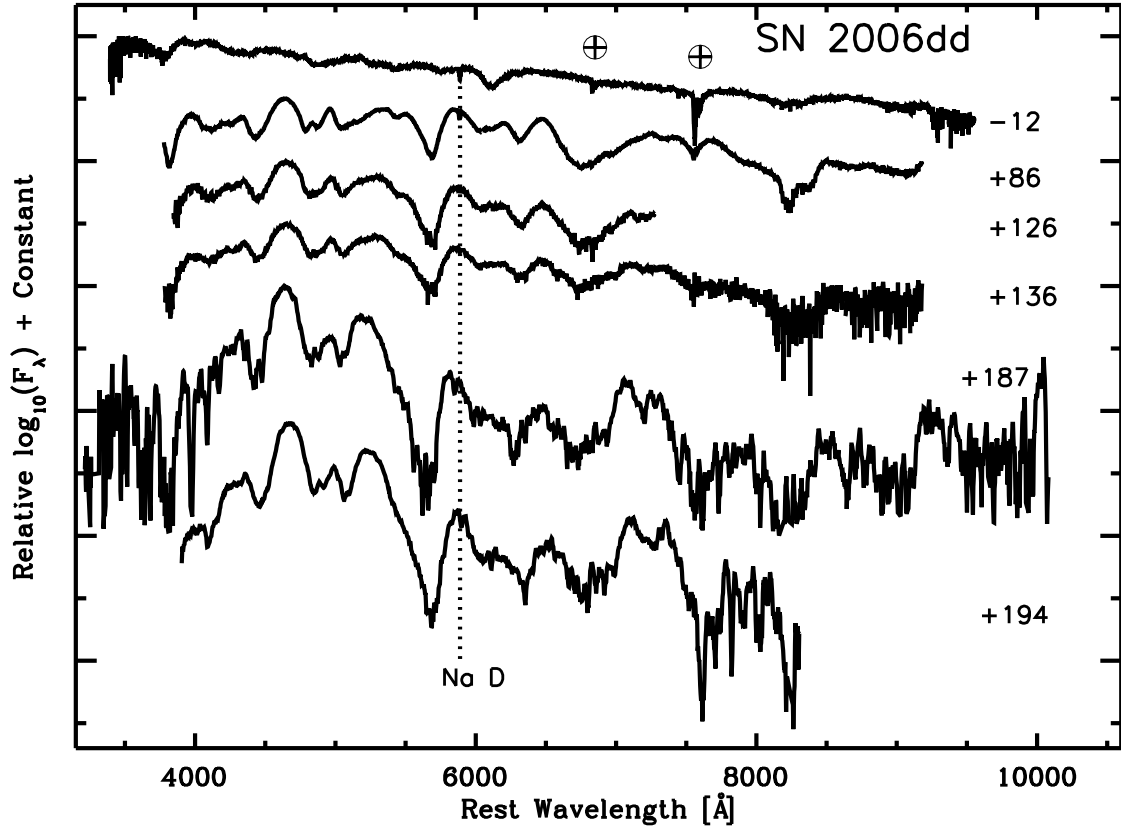


Fig. 2.— Early and late phase optical spectroscopy of SN 2006dd. Telluric features are indicated with an Earth symbol.

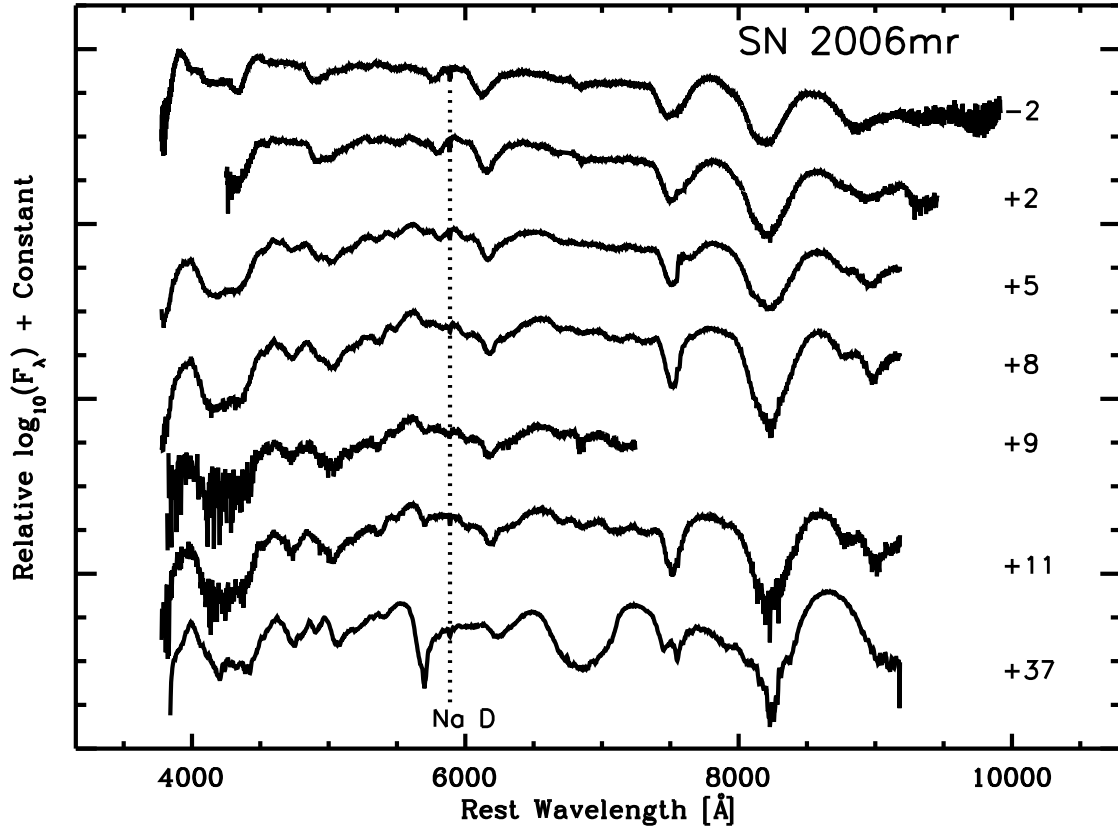


Fig. 3.— Optical spectroscopy of SN 2006mr.



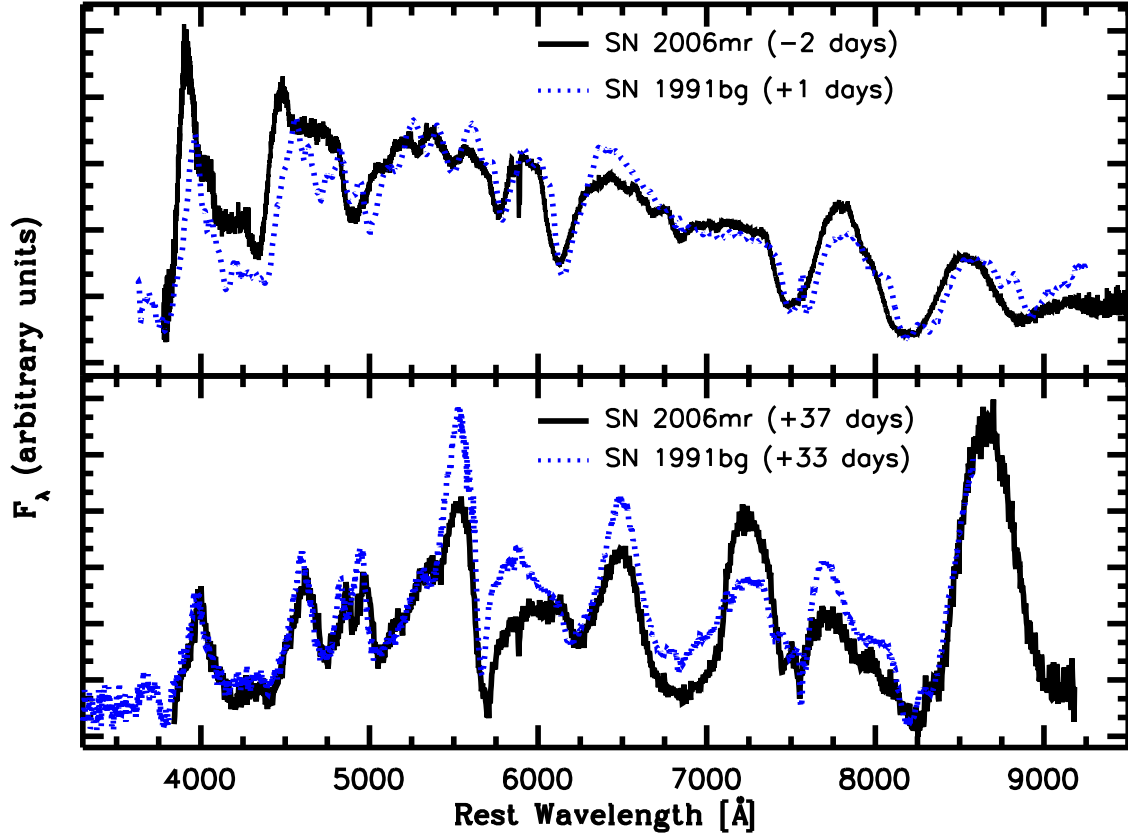


Fig. 4.— Comparison of optical spectra of SN 1991bg and SN 2006mr. The spectra of SN 1991bg are from Turatto et al. (1996) and were obtained from the SUSPECT database.

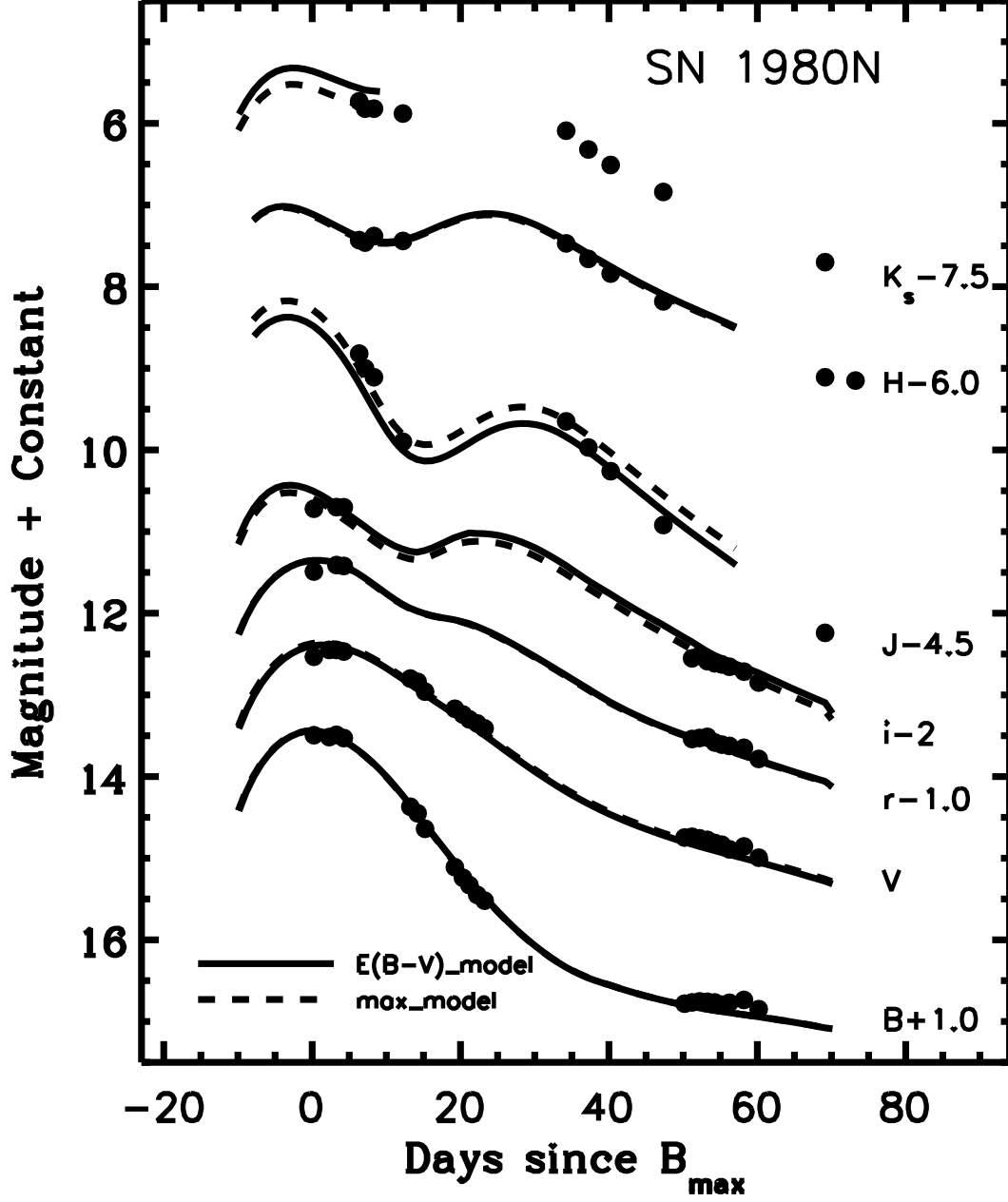


Fig. 5.—  $BVriJHK_s$  light curves of SN 1980N on the natural system of the Swope 1 m telescope. The smooth curves are the best SNooPy “EBV model” fits (solid lines) and the dashed lines correspond to the best “max model” fits. Note that the light curves have been shifted in the y-direction for clarity.

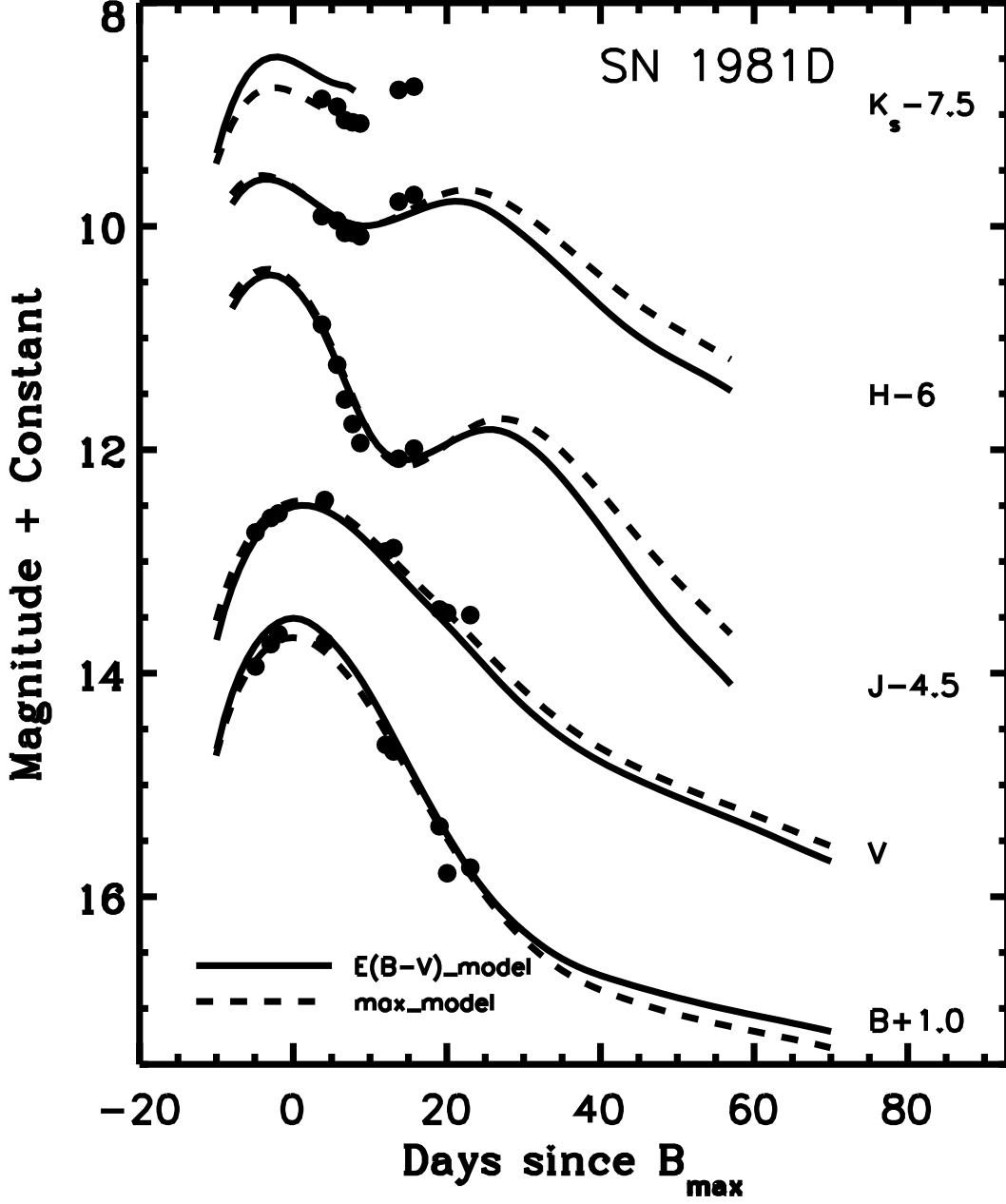


Fig. 6.—  $BVJHK_s$  light curves of SN 1981D on the natural system of the Swope 1 m telescope. The smooth curves are the best SNooPy “EBV model” fits (solid lines) and the dashed lines correspond to the best “max model” fits. Note that the light curves have been shifted in the y-direction for clarity.

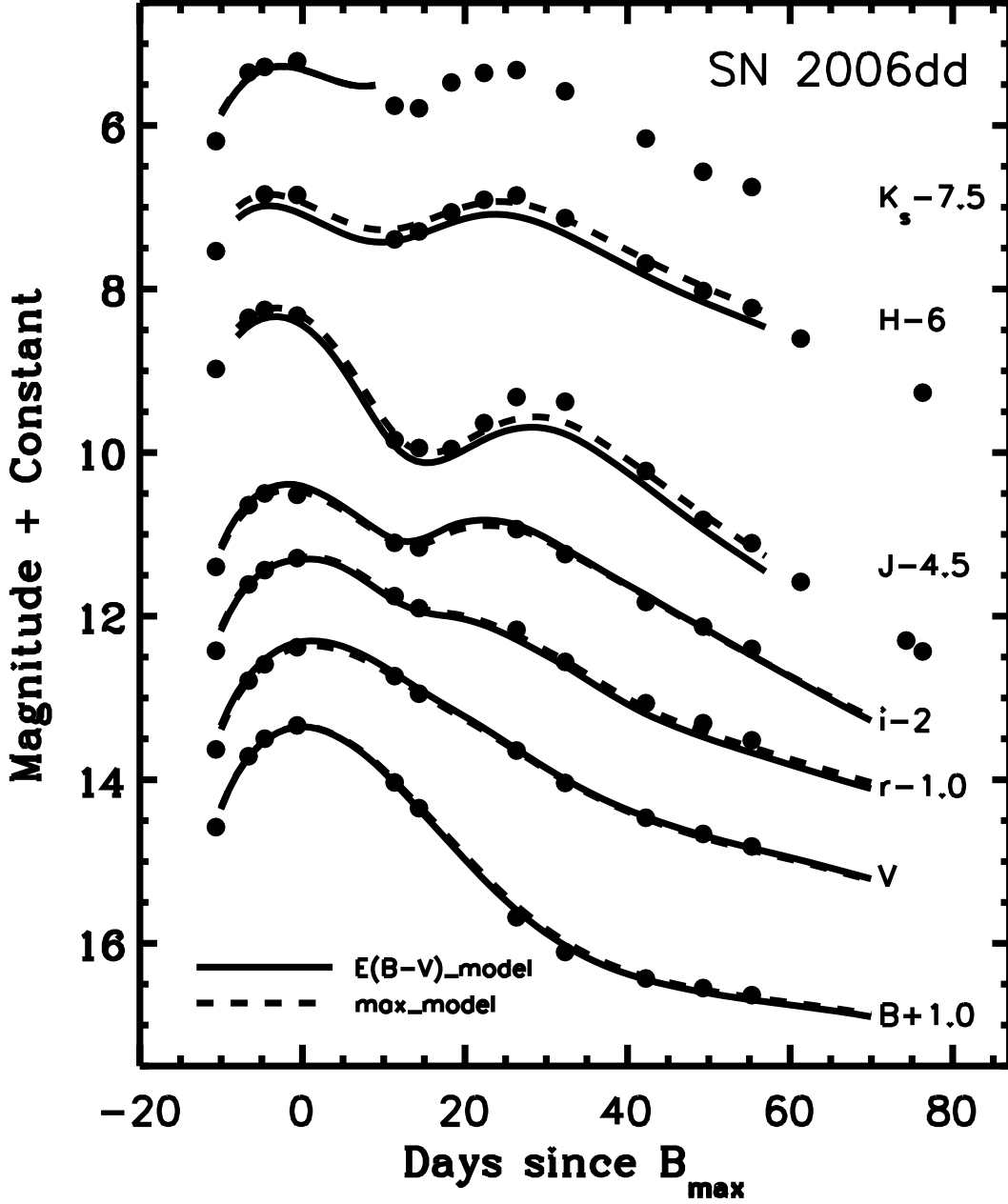


Fig. 7.—  $BVriJHK_s$  light curves of SN 2006dd on the natural system of the Swope 1 m telescope. The smooth curves are the best SNooPy “EBV model” fits (solid lines) and the dashed lines correspond to the best “max model” fits. Note that the light curves have been shifted in the y-direction for clarity.

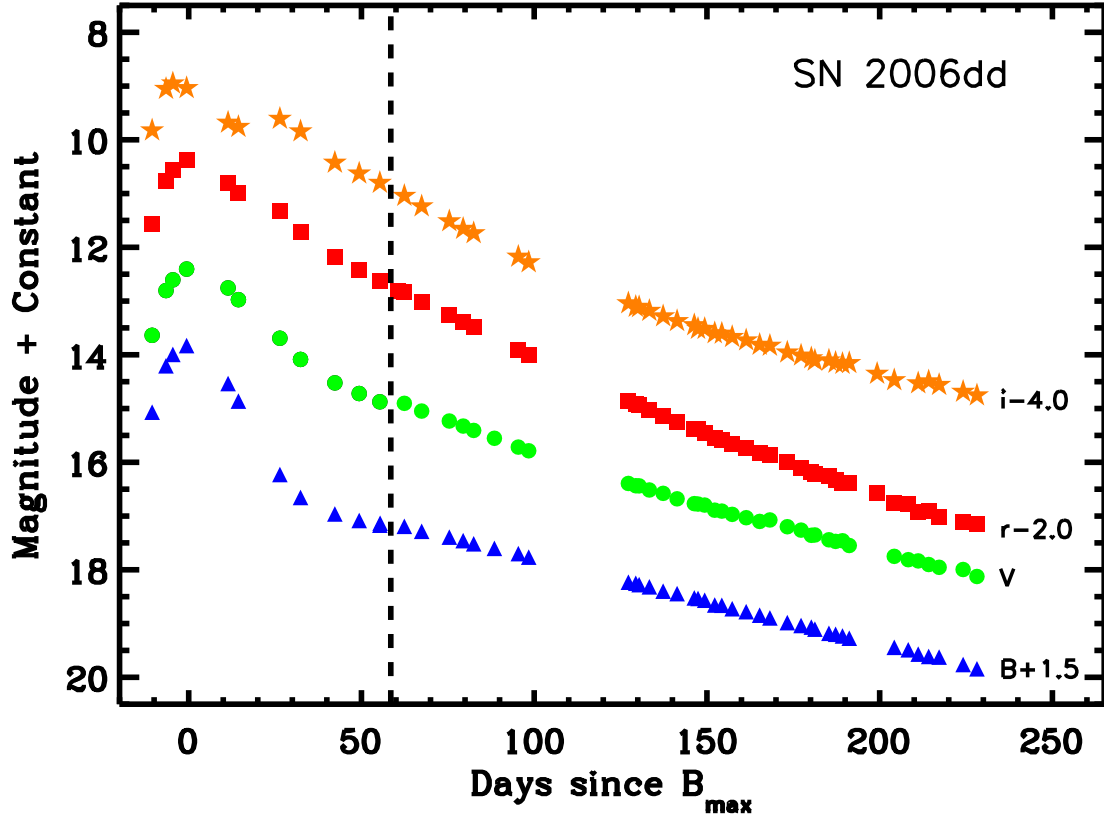


Fig. 8.— Optical  $BVri$  light curves of SN 2006dd on the natural system of the Swope 1 m telescope. The vertical line indicates the epoch between the ANDICAM and Swope photometry. After the application of the S-corrections to the ANDICAM photometry to put it on the natural system of the Swope telescope, the photometry is in excellent agreement with the Swope photometry in the  $Bri$  bands, but less consistent in the  $V$  band.

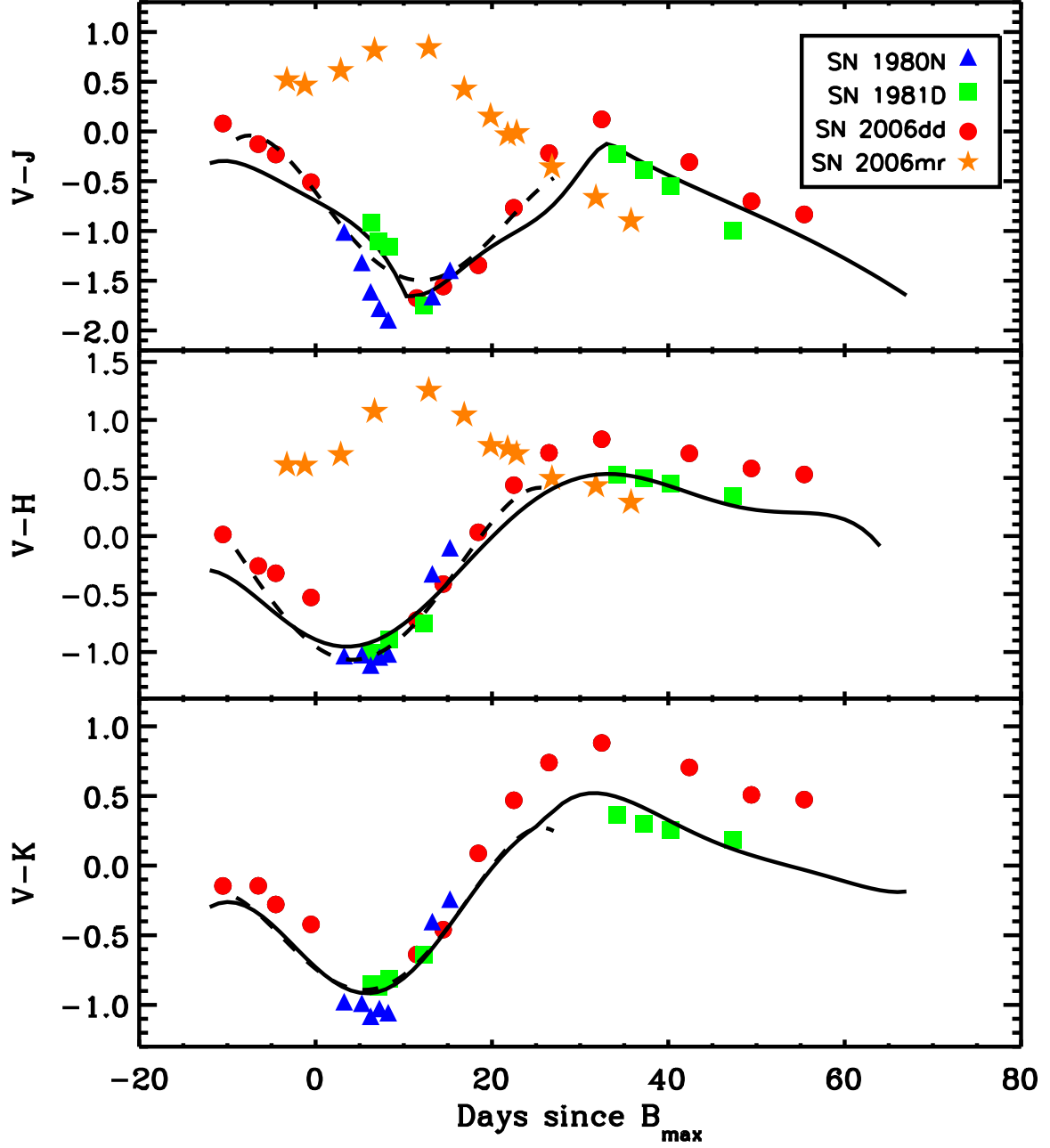


Fig. 9.— Observed  $V$  minus NIR color curves of SN 1980N, SN 1981D, SN 2006dd, and SN 2006mr. The data have been  $K$ -corrected and corrected for Galactic reddening. Solid lines correspond to zero-reddening loci of SN 2001el. For comparison, the loci for midrange decliners is also shown (Krisciunas et al. 2000).

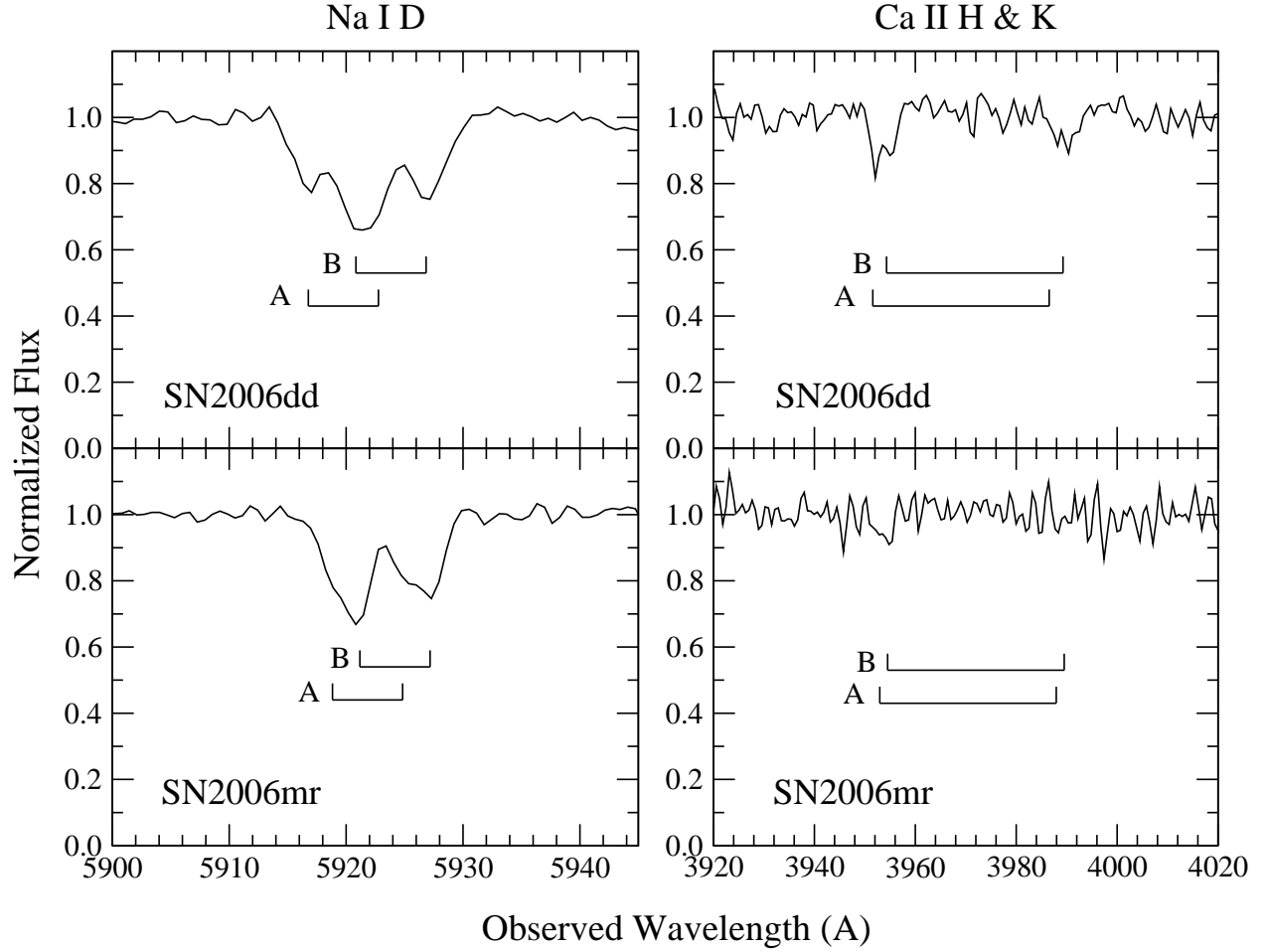


Fig. 10.— Spectra of SNe 2006dd and 2006mr in the region of the interstellar Na I D and Ca II H & K lines in the rest system of NGC 1316. Indicated by the letters “A” and “B” are the two strong systems observed in both SNe. The spectrum of SN 2006dd was obtained on 21 June 2006 with a FWHM resolution of 3.3 Å; that of SN 2006mr was acquired on 09 Nov. 2006 at a resolution of 2.4 Å.

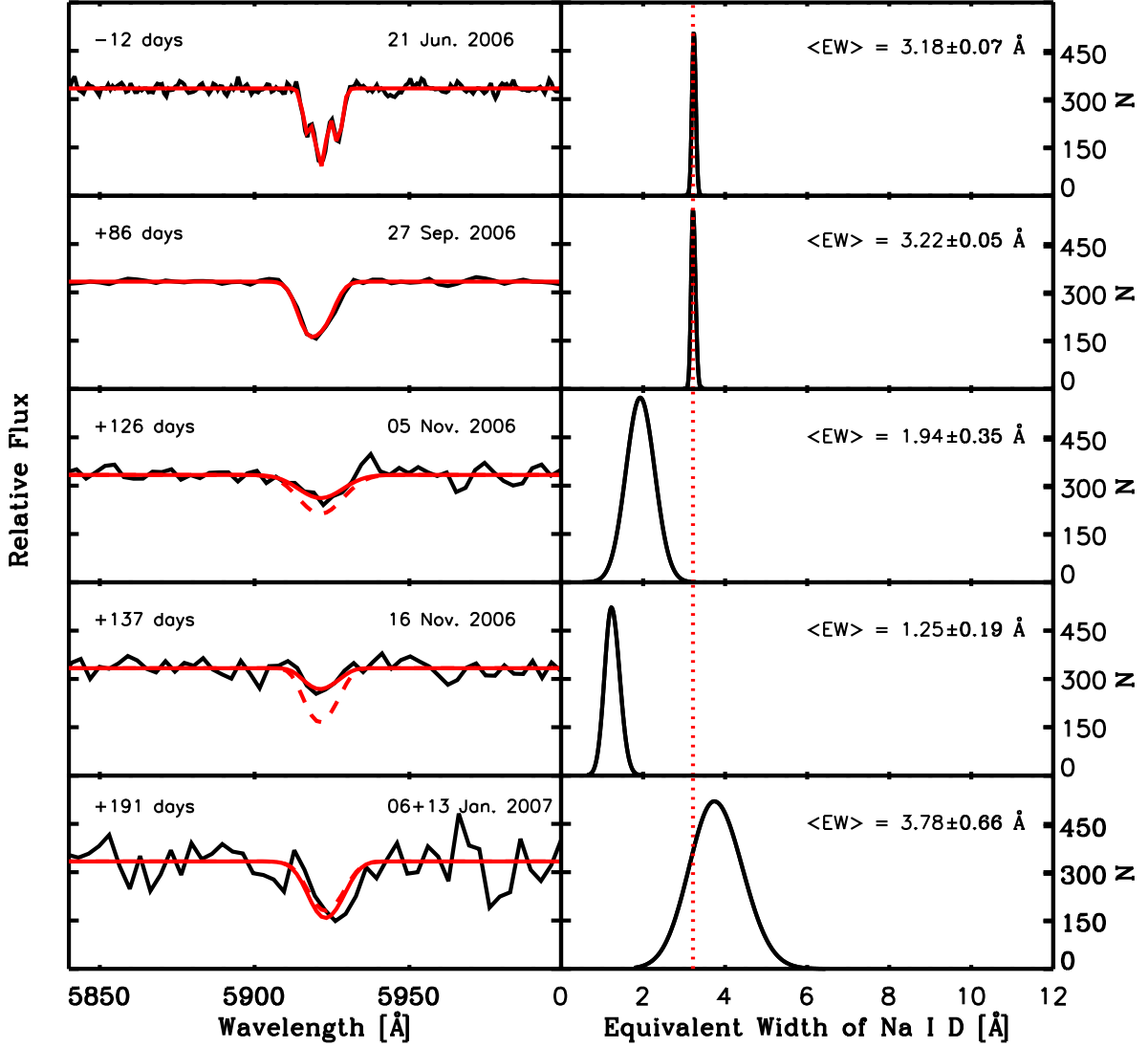


Fig. 11.— (*left*) Evolution of the Na I D interstellar lines in SN 2006dd and (*right*) posterior probability distributions for the total equivalent width values derived from Markov chain Monte Carlo fitting simulations. The best modeled spectra (red solid lines) are overplotted on the observed spectra (black solid lines). In the case of the two spectra obtained on 05 Nov. 2006 and 16 Nov. 2006, we also include the model with a total equivalent width of  $3.2 \text{ \AA}$  (red dashed lines). The final spectrum is actually the sum of two observations made within a week of each other in Jan. 2007. To facilitate comparison of the PPDs, a vertical (red dotted) line has been drawn at  $3.2 \text{ \AA}$  to guide the eye.



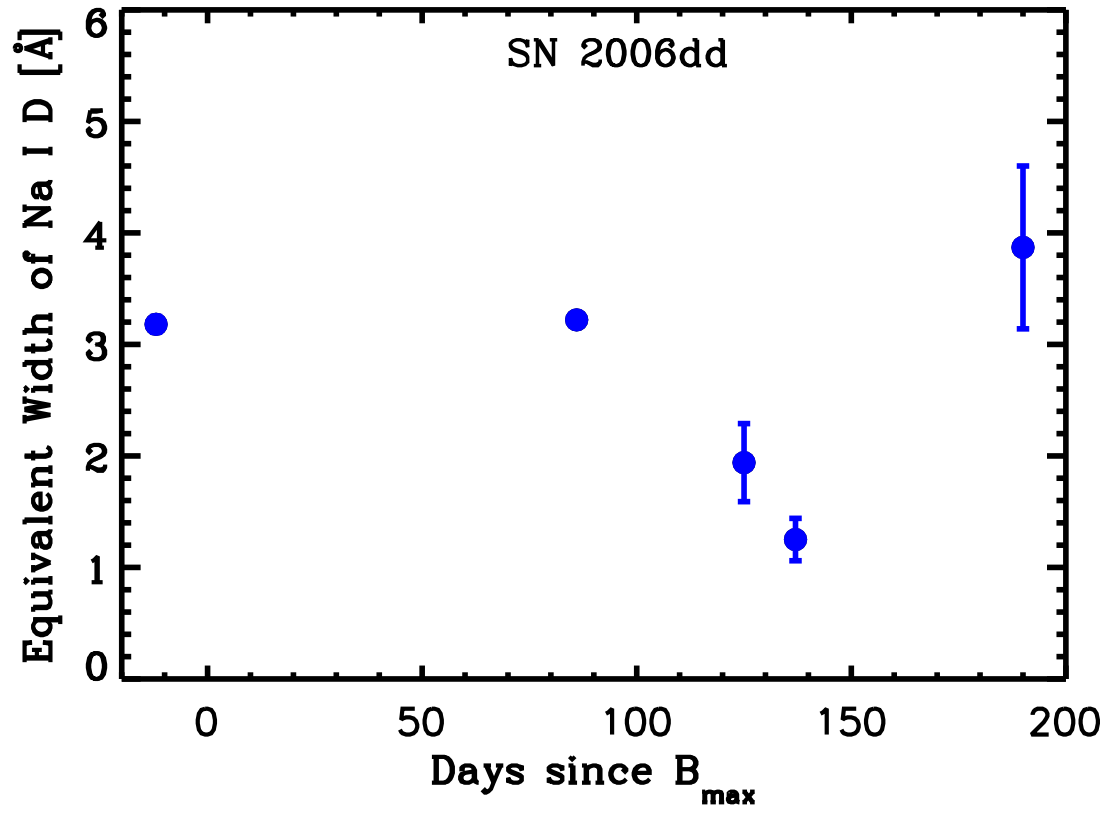


Fig. 12.— Evolution of the Na I D equivalent width in SN 2006dd vs. days past  $B_{\max}$ . Error-bars are  $1\text{-}\sigma$ .

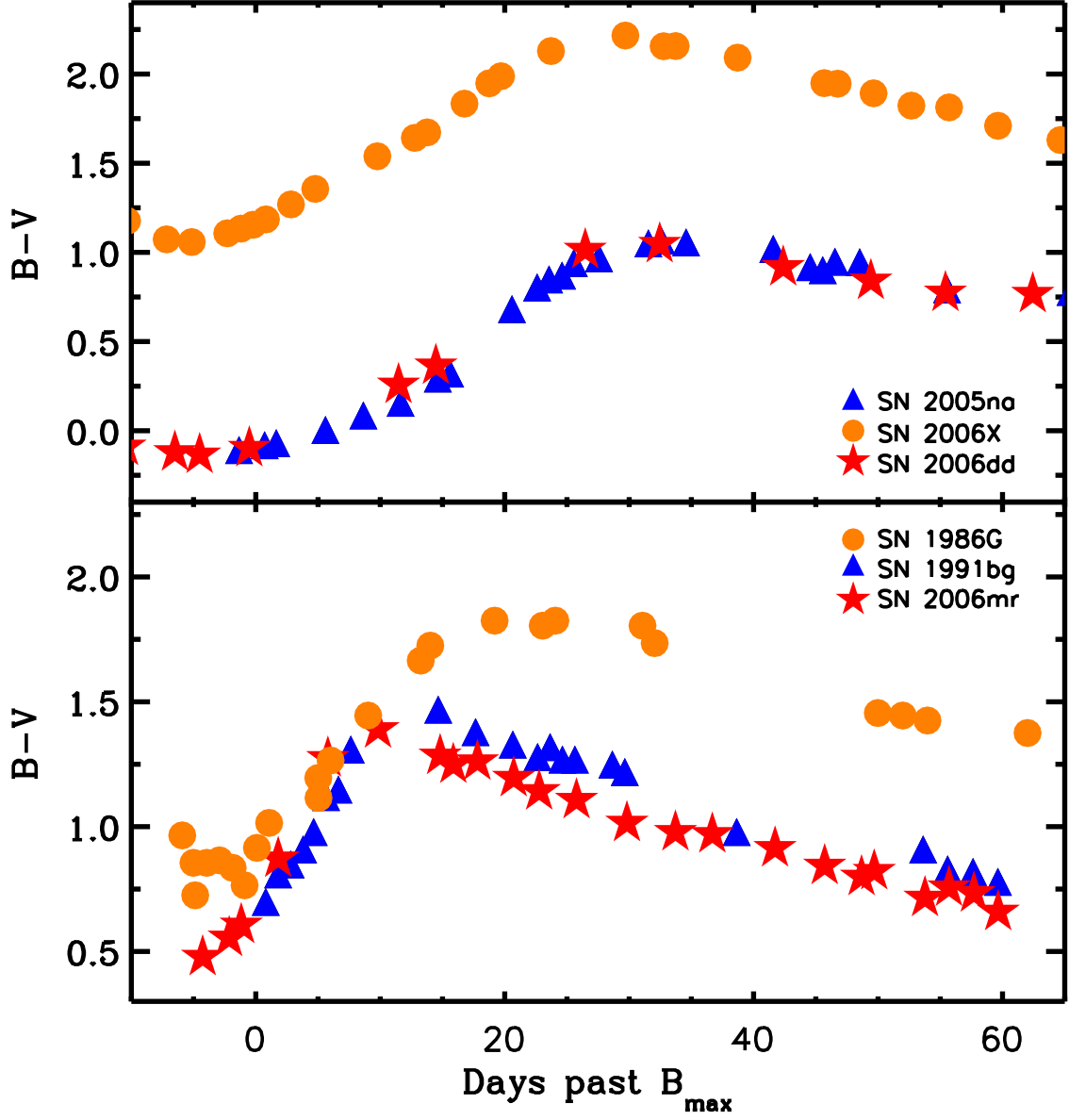


Fig. 13.— Observed  $(B-V)$  color curves of (*top*) normal and (*bottom*) low-luminosity SNe Ia. Photometry of SN 2005na and SN 2006dd is from Contreras et al. (2010), while SN 1986G and SN 1991bg originate from Phillips et al. (1987) and Leibundgut (1993), respectively. Each color curve has been corrected for Galactic reddening.